Summation by parts and truncation error matching on hyperboloidal slices

Shalabh Gautam,[1,*] Alex Vañó-Viñuales,[2] David Hilditch,[2] and Sukanta Bose[1,3]

[1]*Inter-University Centre for Astronomy and Astrophysics, Post Bag 4, Ganeshkhind, Pune 411007, India*
[2]*CENTRA, Departamento de Física, Instituto Superior Técnico IST, Universidade de Lisboa UL, Avenida Rovisco Pais 1, 1049-001 Lisboa, Portugal*
[3]*Department of Physics and Astronomy, Washington State University, Pullman, Washington 99164, USA*

(Received 21 January 2021; accepted 19 February 2021; published 23 April 2021)

We examine stability of summation by parts (SBP) numerical schemes that use hyperboloidal slices to include future null infinity in the computational domain. This inclusion serves to mitigate outer boundary effects and, in the future, will help reduce systematic errors in gravitational waveform extraction. We also study a setup with truncation error matching. Our SBP-Stable scheme guarantees energy balance for a class of linear wave equations at the semidiscrete level. We develop also specialized dissipation operators. The whole construction is made at second-order accuracy in spherical symmetry but could be straightforwardly generalized to higher order or spectral accuracy without symmetry. In a practical implementation, we evolve first a scalar field obeying the linear wave equation and observe, as expected, long-term stability and norm convergence. We obtain similar results with a potential term. To examine the limitations of the approach, we consider a massive field, whose equations of motion do not regularize and whose dynamics near null infinity, which involve excited incoming pulses that cannot be resolved by the code, is very different to that in the massless setting. We still observe excellent energy conservation, but convergence is not satisfactory. Overall, our results suggest that compactified hyperboloidal slices are likely to be provably effective whenever the asymptotic solution space is close to that of the wave equation.

DOI: 10.1103/PhysRevD.103.084045

I. INTRODUCTION

A persistent problem in numerical relativity is the inclusion of future null infinity $\mathscr{I}^+$ in the computational domain. As described by Penrose [1], future null infinity is the set of end points of future directed null geodesics. Ultimately, this will allow us to study the propagation of waves out to $\mathscr{I}^+$. In the modern era of gravitational wave astronomy, one landmark goal is to compute waveforms from a binary merger in a completely satisfactory manner. The present state of the art for extracting signals at $\mathscr{I}^+$ is to use Cauchy-characteristic extraction [2–6]. In this approach, a standard time evolution is performed, and data taken on a timelike worldtube from that evolution serve as the *given data* for a tertiary computation on outgoing characteristic slices compactified to $\mathscr{I}^+$. This approach suffers from the principle weakness that data transfer is one way, so eventually artificial outer boundary conditions in the Cauchy domain corrupt the interior physically correct data. Cauchy-characteristic matching [7] proposes to solve this shortcoming by evolving and coupling both domains simultaneously. In practice, interfacing two different formulations of general relativity (GR) may not, however, result in a composite partial differential equation problem that is well posed [8].

An alternative path, which we follow, is to use compactified hyperboloidal slices, which are everywhere spacelike but which terminate at $\mathscr{I}^+$. Starting with the conformal field equations [9,10], hyperboloidal slices have been used with several formulations of GR [11–16], all of which have to render the field equations sufficiently regular for numerical approximation in some way. The specific strategy we follow was suggested in Ref. [17] and employs the dual foliation (DF) formalism [18]. The means to achieve regular equations for regular unknowns is to use a carefully chosen tensor basis in combination with hyperboloidal coordinates. Follow-ups on the mathematical formalism [19] and numerical implementation [20] have shown that it should be possible to manage logarithmic divergences that appear in the asymptotic solution space by a careful choice of variables.

Until now, our analysis [17,19,20] has always been performed at the continuum level, with verification of convergence of numerical schemes being performed only empirically. Thus, the question arises whether a numerical scheme can be given that provably converges to the continuum solution in the limit of infinite resolution. This question is far too difficult to tackle right away for GR. Even for systems used in the perturbative studies [21,22], there is no rigorous numerical analysis. In this paper, we therefore deal with the simplest case of a scalar

*shalabh@iucaa.in

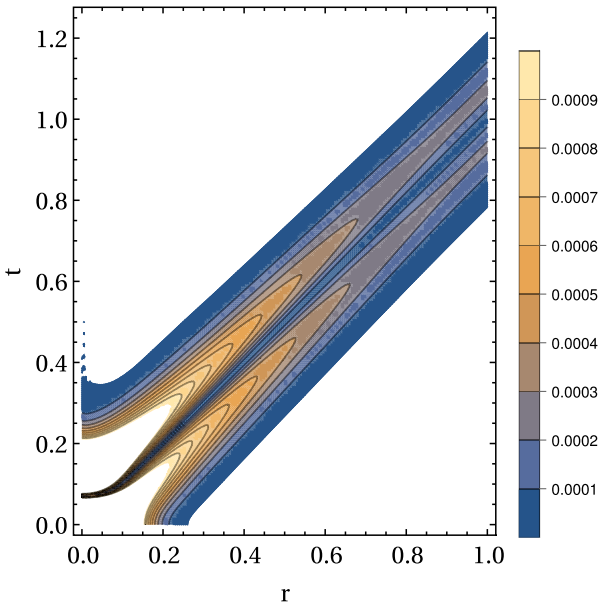

FIG. 1. A contour plot showing the propagation of a pulse of a scalar field $\tilde{\psi}$, satisfying the wave equation, propagating to $\mathcal{I}^+$, located here at $r = 1$. The solution is computed using our SBP-Stable scheme. The plot is cut off at low and high amplitudes.

field obeying a linear wave equation with potential (LWEP). Special cases occur when the potential vanishes (LWE) and for the massive Klein-Gordon equation (LMKGE). We build two approximation schemes. In some sense, both use a summation by parts (SBP) approach [23]. The first, which we call SBP-Stable, is formally stable and captures at the semidiscrete level the energy conservation properties of the continuum system. In the second scheme, which we call SBP-TEM, we apply truncation error matching (TEM) at $\mathcal{I}^+$ (see, for example, Ref. [24]) rather than accepting the lower-order accurate pointwise approximation that is unfortunately necessary in the first approach. This helps minimize unphysical reflections from the outer boundary. We work at second-order accuracy on a Minkowski background. In this work, we restrict ourselves to spherical symmetry. Technical difficulties arise because of the coordinate singularity at the origin, but the key challenge we face is in managing the asymptotics near $\mathcal{I}^+$. We fully expect a generalization of our scheme to hold in more general scenarios. In Fig. 1, we present a contour plot of a numerical solution for the wave equation, in which one can see that the pulse leaves the domain in essentially two bursts, with no visible numerical reflection.

It is intuitively clear that to reach $\mathcal{I}^+$ some price must be paid. By construction, our coordinates are well adapted to outgoing radiation, but there is a key difficulty in resolving *incoming* waves. To investigate this, we perform tests with different potentials, that result in a coupling between outgoing and incoming pulses. Of particular interest is the LMKGE. It turns out that compactification makes the mass term singular at $\mathcal{I}^+$. But as described by Winicour [25] solutions fall off toward $\mathcal{I}^+$ faster than any inverse power of areal radius R, so the field decays more rapidly toward $\mathcal{I}^+$ than the rate at which the coefficient of the mass term blows up. With this setup, our scheme guarantees perfect energy conservation, but we find that the excitation of badly resolved incoming pulses prevents long-term convergence. In practice, this means that, at least for now, if one wishes to use massive fields with hyperboloidal slices, we need to keep the support of the fields away from the wave zone. Working with less aggressive potentials, we find that perfect long-term convergence is, as expected, immediately recovered.

The paper is structured as follows. In Sec. II, we begin with a summary of the specific hyperboloidal foliation that we use. The foliation can be adjusted with only superficial changes to the subsequent expressions. In Sec. III, we present our model equation and derive an appropriate energy-balance law on hyperboloidal slices for the continuum equations. Building directly on this, in Sec. IV, we construct our SBP schemes, leaving some technical parts for the Appendixes. Afterward, in Sec. V, numerical evolutions are presented with a series of different potentials. Finally, we conclude in Sec. VI. Geometric units are used throughout.

II. HYPERBOLOIDAL SLICES OVERVIEW

We now briefly review geometric quantities describing a foliation of spacetime, for which we use the standard notation, and evaluate them under our choice of hyperboloidal slices. They will be used to obtain an energy on such slices conserved up to boundary fluxes, which will, in turn, underpin our numerical scheme. Let $x^{\underline{\mu}'} = (T, R, \theta^A)$ be the canonical spherical polar coordinates on the Minkowski spacetime, so that the line element becomes

$$ds^2 = -dT^2 + dR^2 + R^2 d\Omega^2, \tag{1}$$

where $d\Omega^2$ is the line element on the unit round two-sphere. Let $x^\mu = (t, r, \theta^A)$ be the hyperboloidal coordinates, defined by $T = t + H(R)$ and $R = R(r)$. Here, $r \in [0, r_{\mathcal{I}}]$ is a compactified radial coordinate with $r_{\mathcal{I}}$ a fixed positive number that denotes the value of r at $\mathcal{I}^+$. The angular coordinates θ^A are held fixed.

Let $C^R_\pm = \pm 1$ denote the outgoing and incoming radial light speeds in the original coordinates, and $c^r_\pm$ those in hyperboloidal coordinates. For the latter, we get

$$c^r_\pm = \pm \frac{1}{R'(1 \mp H')}, \tag{2}$$

with $H' \equiv dH/dR$ and $R' \equiv dR/dr$. Thus, the light speeds $c^r_\pm$ are functions of r. If we choose R and H carefully, we can restrict these functions to a desired form. Ideally, we would have $c^r_\pm = \pm 1$ so that both incoming and outgoing pulses could be resolved. However, this is not completely compatible with our wish to draw infinity to a finite

coordinate distance by use of a compactification $R(r)$. In particular, following Ref. [26], we might take the simple

$$R(r) = \frac{r}{\Omega(r)^{1/(1-n)}} = r\left(1 - \frac{r^2}{r_{\mathscr{J}}^2}\right)^{1/(1-n)}, \tag{3}$$

with $1 < n \leq 2$ and $r \in [0, r_{\mathscr{J}}]$. Later, we adjust to a slightly different compactification. With this choice, $R' \sim R^n$ as $r \to r_{\mathscr{J}}$. Thus, only the height function H remains to be chosen. To resolve outgoing pulses, of primary interest in the asymptotically flat setting, we thus choose H so that $c_+^r = 1$. Throughout, we choose $R'(1 - H') = 1$, or $H' = 1 - 1/R'$, and, thus, obtain $c_+^r = 1$ identically, and $c_-^r = -1/(2R' - 1)$. Note that $c_-^r = -1$ at the origin and decreases in magnitude monotonically to 0 at $r_{\mathscr{J}}$. The line element becomes

$$ds^2 = -dt^2 - 2(R' - 1)dtdr + (2R' - 1)dr^2 + R^2 d\Omega^2. \tag{4}$$

The components of the spatial metric γ_{ij} here can be read off from the spatial components. The lapse α and only nontrivial component of the shift β^i are given, respectively, by

$$\alpha = R'(2R' - 1)^{-(1/2)}, \qquad \beta^r = -\frac{R' - 1}{2R' - 1}. \tag{5}$$

Note that the shift is negative but finite near and at $\mathscr{J}$. Finally, the extrinsic curvature K_{ab} can be computed from $\mathcal{L}_t \gamma_{ab} = 0$ but is not explicitly needed in the following.

III. THE WAVE EQUATION WITH POTENTIAL ON HYPERBOLOIDAL SLICES

In this section, we formulate the LWE with a linear potential F on our hyperboloidal slices and study its regularization. The case of the LWE can be obtained simply by taking $F = 0$.

A. The wave equation and regularity at the origin

Consider a scalar field ψ satisfying a linear wave equation with a potential F:

$$(\Box - F)\psi = 0, \tag{6}$$

where $\Box$ is the standard d'Alembertian. Imposing spherical symmetry, we require that $\psi = \psi(T, R)$ and also that the potential be time independent and non-negative, i.e., $F = F(R) \geq 0$. Defining $\pi \equiv -\partial_T \psi$ and $\phi_R \equiv \partial_R \psi$, we thus get a first-order reduction of this equation in the form of a system of three first-order equations in three variables:

$$\begin{aligned} \partial_T \psi &= -\pi, \\ \partial_T \phi_R &= -\partial_R \pi + \gamma_2(\partial_R \psi - \phi_R), \\ \partial_T \pi &= -\partial_R \phi_R - \frac{2}{R}\phi_R + F\psi. \end{aligned} \tag{7}$$

The first equation comes directly from the definition of π. The second follows by equality of mixed partials ∂_T and ∂_R. The γ_2 coefficient serves to damp the reduction constraints [27,28] associated with the definition of ϕ_R. This constraint vanishes at the continuum level in the original second-order system but should not be assumed to necessarily vanish in the reduction or, in general, at the discrete level. Later, we will choose $\gamma_2 = 0$ and will study conditions under which the constraint is satisfied, in some sense, even at the discrete level. The third equation is obtained by substituting for $\partial_T \psi$ and $\partial_R \psi$ within Eq. (6).

Following the dual foliation [18] strategy of our earlier work [17,19,20], we rewrite this first-order reduction system in hyperboloidal coordinates while keeping the reduction variables (ψ, ϕ_R, π) unchanged. This approach has the technical advantage that the same dynamical variables are evolved in two coordinate systems. Changing to the coordinates x^μ introduced in Sec. II, Eqs. (7) become

$$\begin{aligned} \partial_t \psi &= -\pi, \\ \partial_t \phi_R &= -\frac{R'}{2R' - 1}\partial_r \pi - \frac{R' - 1}{2R' - 1}\left[\partial_r + \frac{2R'}{R}\right]\phi_R \\ &\quad + \frac{\gamma_2 R'}{2R' - 1}[\partial_r \psi + (R' - 1)\pi - R'\phi_R] + \frac{R'(R' - 1)}{2R' - 1}F\psi, \\ \partial_t \pi &= -\frac{R' - 1}{2R' - 1}\partial_r \pi - \frac{R'}{2R' - 1}\left[\partial_r + \frac{2R'}{R}\right]\phi_R \\ &\quad + \frac{\gamma_2(R' - 1)}{2R' - 1}[\partial_r \psi + (R' - 1)\pi - R'\phi_R] \\ &\quad + \frac{R'^2}{2R' - 1}F\psi. \end{aligned} \tag{8}$$

The origin of the γ_2 terms appearing above is the single constraint equation introduced in Eqs. (7), expressed here in lowercase coordinates. Regularity at the origin is well understood, but as it will play an important role in our numerical scheme we nevertheless provide a brief discussion about it. Since we are working in spherical symmetry, we will substitute the θ and ϕ coordinates by $\theta^A = (\theta, \phi)$. The radial coordinate goes from 0 to $r_{\mathscr{J}}$. The origin is not a physical boundary but the artifact of the choice of spherical coordinates. The terms containing $1/R$ become singular as $R \to 0$, but the $1/R$ coefficient appears multiplying only ϕ_R, which must vanish for $r \to 0$. This is due to regularity at the origin. If we were to extend all three variables (ψ, ϕ_R, π) from $[0, r_{\mathscr{J}}]$ to $[-r_{\mathscr{J}}, r_{\mathscr{J}}]$ (equivalent to considering positive r at $\phi \to \phi + \pi$), parity of the fields requires that ψ and π (scalars) be even functions of r and ϕ_R, as the radial derivative of a scalar, be an odd function. The result is that $\partial_t \phi_R = 0$ at the origin for all times. Applying l'Hôpital's rule gives $\phi_R/R \to \phi_R'/R'$ as $r \to 0$, and the equations at the origin become

$$\begin{aligned}\partial_t\psi(t,0) &= -\pi(t,0),\\ 0 &= -\partial_r\pi(t,0),\\ \partial_t\pi(t,0) &= -3\phi_R'(t,0) + F\psi(t,0),\end{aligned} \tag{9}$$

both in canonical spherical polars and in hyperboloidal coordinates. The γ_2 terms vanish because, due to the parity condition above, $\partial_r\psi = 0$ and $\phi_R = 0$ at the origin, while $R' - 1 = 0$ at the origin by definition. The second equation, therefore, gives just an identity.

Equations (8), which use hyperboloidal coordinates, can be rewritten in terms of the incoming and outgoing characteristic variables

$$\sigma^+ \equiv -\pi + \phi_R, \qquad \sigma^- \equiv -\pi - \phi_R, \tag{10}$$

respectively, resulting in

$$\begin{aligned}\partial_t\psi &= \frac{1}{2}(\sigma^+ + \sigma^-),\\ \partial_t\sigma^+ &= \frac{1}{2R'-1}\left[\partial_r\sigma^+ + \frac{R'}{R}(\sigma^+ - \sigma^-) - R'F\psi\right]\\ &\quad + \gamma_2\left[\frac{1}{2R'-1}\left(\partial_r\psi + \frac{\sigma^-}{2}\right) - \frac{\sigma^+}{2}\right],\\ \partial_t\sigma^- &= -\left[\partial_r\sigma^- + \frac{R'}{R}(\sigma^- - \sigma^+) + R'F\psi\right]\\ &\quad - \gamma_2\left[\left(\partial_r\psi + \frac{\sigma^-}{2}\right) - (2R'-1)\frac{\sigma^+}{2}\right].\end{aligned} \tag{11}$$

Here again, the γ_2 terms are proportional to the reduction constraint. The equivalent transformation for the flat equations (7) can be straightforwardly obtained from Eqs. (11) by substituting $R' \to 1$, $r \to R$, and $t \to T$.

From Eqs. (11), we see that

$$\phi_R(t,0) = 0 \Rightarrow \sigma^+(t,0) = \sigma^-(t,0) = -\pi(t,0) \tag{12}$$

and

$$\partial_r\pi(t,0) = 0 \Rightarrow \partial_r\sigma^+(t,0) = -\partial_r\sigma^-(t,0) = \partial_r\phi_R(t,0), \tag{13}$$

yielding

$$\begin{aligned}&\partial_t\psi(t,0) = \sigma^+(t,0) = \sigma^-(t,0),\\ &\partial_t\sigma^+(t,0) = -3\partial_r\sigma^-(t,0) - F\psi(t,0),\\ &\partial_t\sigma^-(t,0) = -3\partial_r\sigma^-(t,0) - F\psi(t,0) = \partial_t\sigma^+(t,0),\end{aligned} \tag{14}$$

in both flat and hyperboloidal coordinates. The last equation makes sense, because $\sigma^+(t,0) = \sigma^-(t,0)$ for all times t.

B. Regularization

We now look at the behavior of the solutions near $\mathscr{I}^+$ and examine how it may be used to regularize terms appearing in the field equations with R'. For example, in Eqs. (11), $(R'/R)\phi_R$ and potential terms appear, with coefficients that become singular at $r_{\mathscr{I}}$. But, on the other hand, we expect that the field variables (ψ, ϕ_R, π) fall off as positive powers of $1/R$ when $r \to r_{\mathscr{I}}$. Thus, in order to regularize these terms, we seek a suitable rescaling of the field variables. The expectation is that the presence of a physically reasonable potential does not induce slower decay toward $\mathscr{I}^+$ than for a solution of the LWE. Therefore, we rescale our variables according to expected decay rates for the LWE regardless of the form of F, to be set later on.

1. (ψ, ϕ_R, π) variables

A scalar field ϕ obeying the LWE falls off like $1/R$ toward $\mathscr{I}^+$. This suggests the rescaling

$$\tilde{\psi} \equiv \chi\psi, \qquad \tilde{\phi}_R \equiv \chi\phi_R + \chi'\psi, \qquad \tilde{\pi} \equiv \chi\pi, \tag{15}$$

with $\chi = \chi(R) \simeq R$ for large R and $\chi \simeq 1$ near the origin. These conditions ensure that the equations are unaffected at the origin but that the evolved variables become $O(1)$ at $\mathscr{I}^+$. As in Ref. [20], we take $\chi \equiv \sqrt{1+R^2}$. The system satisfies

$$\begin{aligned}\partial_t\tilde{\psi} &= -\tilde{\pi},\\ \partial_t\tilde{\phi}_R &= -\frac{R'}{2R'-1}\partial_r\tilde{\pi} - \frac{R'-1}{2R'-1}\partial_r\tilde{\phi}_R - \frac{2R'(R'-1)}{(2R'-1)\chi^2 R}\tilde{\phi}_R\\ &\quad + \frac{R'(R'-1)}{2R'-1}\left(\frac{3}{\chi^4} + F\right)\tilde{\psi} + \frac{\gamma_2 R'}{2R'-1}[\partial_r\tilde{\psi}\\ &\quad + (R'-1)\tilde{\pi} - R'\tilde{\phi}_R],\\ \partial_t\tilde{\pi} &= -\frac{R'-1}{2R'-1}\partial_r\tilde{\pi} - \frac{R'}{2R'-1}\partial_r\tilde{\phi}_R - \frac{2R'^2}{(2R'-1)\chi^2 R}\tilde{\phi}_R\\ &\quad + \frac{R'^2}{2R'-1}\left(\frac{3}{\chi^4} + F\right)\tilde{\psi} + \frac{\gamma_2(R'-1)}{2R'-1}[\partial_r\tilde{\psi}\\ &\quad + (R'-1)\tilde{\pi} - R'\tilde{\phi}_R].\end{aligned} \tag{16}$$

The potential term remains singular at $r_{\mathscr{I}}$ if F does not fall faster than $1/R$. If at large R we have $F \sim 1/R^{1+\epsilon}$, with $\epsilon > 0$, we can choose n in Eq. (3) such that $1 < n < 1 + \epsilon$, which gives $R'F \to 0$ as $r \to r_{\mathscr{I}}$ and the term becomes regular. The constraint damping terms are also tricky, since, at least naively, they require γ_2 to fall off very fast.

2. $(\psi, \sigma^+, \sigma^-)$ variables

A change of variables that captures more sharply the falloff of solutions and that generalizes to nonlinear systems by the use of asymptotic expansions [29,30] is offered by

$$\tilde{\psi} \equiv \chi\psi, \qquad \tilde{\sigma}^+ \equiv \chi^2\sigma^+, \qquad \tilde{\sigma}^- \equiv \chi\sigma^-. \tag{17}$$

These variables satisfy the equations of motion

$$\begin{aligned}
\partial_t\tilde{\psi} &= \frac{1}{2}\left[\frac{\tilde{\sigma}^+}{\chi} + \tilde{\sigma}^-\right],\\
\partial_t\tilde{\sigma}^+ &= \frac{1}{2R'-1}\left[\partial_r\tilde{\sigma}^+ - \frac{2RR'}{\chi^2}\tilde{\sigma}^+ + \frac{R'}{R}(\tilde{\sigma}^+ - \chi\tilde{\sigma}^-)\right.\\
&\quad \left. - R'\chi F\tilde{\psi}\right] + \gamma_2\left[\frac{1}{2R'-1}\left(\chi\partial_r\tilde{\psi} - \frac{RR'}{\chi}\tilde{\psi} + \chi\frac{\tilde{\sigma}^-}{2}\right) - \frac{\tilde{\sigma}^+}{2}\right],\\
\partial_t\tilde{\sigma}^- &= -\partial_r\tilde{\sigma}^- + \left(\frac{RR'}{\chi^2} - \frac{R'}{R}\right)\tilde{\sigma}^- + \frac{R'}{R\chi}\tilde{\sigma}^+ - R'F\tilde{\psi}\\
&\quad - \gamma_2\left[\partial_r\tilde{\psi} - \frac{RR'}{\chi^2}\tilde{\psi} + \frac{\tilde{\sigma}^-}{2} - (2R'-1)\frac{\tilde{\sigma}^+}{2\chi}\right],
\end{aligned} \tag{18}$$

in hyperboloidal coordinates. As before, the potential term can be regularized only if $F \sim 1/R^{1+\epsilon}$, with $\epsilon > 0$, for large R. Otherwise, all terms, except the second on the right-hand side of the third equation, are regular at $r_{\mathscr{I}}$. A closer inspection, however, shows that these two singular terms, in fact, cancel each other at $\mathscr{I}^+$, rendering the equations regular. Regularity at the origin follows by the same considerations as in the previous section. The regularization scheme for the $(\psi, \sigma^+, \sigma^-)$ system is sharper and simpler than that for the (ψ, ϕ_R, π) variables and is, thus, preferred for numerical work. Other advantages are that the γ_2 constraint terms are regular with no further thought, and, as we shall see, the energy norm it provides is simpler than that of the (ψ, ϕ_R, π) system.

Inspired by Refs. [31–33], for later application in our numerical setup, we define the operator $\tilde{\partial}_r$ as

$$\tilde{\partial}_r\phi \equiv \chi^2(\partial_r + 2R'/R)(\phi/\chi^2). \tag{19}$$

Using this operator, we can avoid the explicit appearance of the term $2R'/R$ which is singular at $r_{\mathscr{I}}$, as $\tilde{\partial}_r$ corresponds to

$$\tilde{\partial}_r\phi = \partial_r\phi + \frac{2R'}{(1+R^2)R}\phi. \tag{20}$$

The motivation behind using this operator will become even more apparent in the next section. With this definition, we can write

$$R'/R = \frac{1}{2}(\chi^{-2}\tilde{\partial}_r\chi^2 - \partial_r). \tag{21}$$

Substituting in Eqs. (18) yields

$$\begin{aligned}
\partial_t\tilde{\psi} &= \frac{1}{2}\left[\frac{\tilde{\sigma}^+}{\chi} + \tilde{\sigma}^-\right],\\
\partial_t\tilde{\sigma}^+ &= \frac{1}{2R'-1}\left[\left(\frac{\partial_r + \tilde{\partial}_r}{2}\right)\tilde{\sigma}^+ + \chi\left(\frac{\partial_r - \tilde{\partial}_r}{2}\right)\tilde{\sigma}^-\right.\\
&\quad \left. - \frac{RR'}{\chi^2}\tilde{\sigma}^+ - \frac{RR'}{\chi}\tilde{\sigma}^- - R'\chi F\tilde{\psi}\right] + \gamma_2\left[\frac{1}{2R'-1}\right.\\
&\quad \left.\times\left(\chi(\partial_r\tilde{\psi}) - \frac{R}{\chi}R'\tilde{\psi} + \chi\frac{\tilde{\sigma}^-}{2}\right) - \frac{\tilde{\sigma}^+}{2}\right],\\
\partial_t\tilde{\sigma}^- &= -\left[\left(\frac{\partial_r + \tilde{\partial}_r}{2}\right)\tilde{\sigma}^- + \left(\frac{\partial_r - \tilde{\partial}_r}{2\chi}\right)\tilde{\sigma}^+\right.\\
&\quad \left. - \frac{RR'}{\chi^3}\tilde{\sigma}^+ + R'F\tilde{\psi}\right] - \gamma_2\left[\partial_r\tilde{\psi} - \frac{R}{\chi^2}R'\tilde{\psi}\right.\\
&\quad \left. + \frac{\tilde{\sigma}^-}{2} - (2R'-1)\frac{\tilde{\sigma}^+}{2\chi}\right].
\end{aligned} \tag{22}$$

At $r_{\mathscr{I}}$, setting $\gamma_2 \simeq 1/R$, the equations take the form

$$\begin{aligned}
\partial_t\tilde{\psi} &= \frac{\tilde{\sigma}^-}{2},\\
\partial_t\tilde{\sigma}^+ &= -\frac{\tilde{\sigma}^-}{2} - \frac{\chi F\tilde{\psi}}{2},\\
\partial_t\tilde{\sigma}^- &= -\left[\left(\frac{\partial_r + \tilde{\partial}_r}{2}\right)\tilde{\sigma}^- - \frac{R'}{\chi^2}\tilde{\sigma}^+ + R'F\tilde{\psi}\right]\\
&\quad - \gamma_2\left[-\frac{R'}{\chi}\tilde{\psi} - (2R'-1)\frac{\tilde{\sigma}^+}{2\chi}\right].
\end{aligned} \tag{23}$$

Again, we see that the potential terms are singular at $r_{\mathscr{I}}$, unless $F \sim 1/R^{1+\epsilon}$, with $\epsilon > 0$, for large R.

C. Conserved energy on hyperboloidal slices

As we saw in the equations of motion, if F falls off too slowly, it may result in singular equations near $\mathscr{I}^+$, even when working with the rescaled variables. A classical example is $F = m^2$, corresponding to the massive Klein-Gordon equation. As pointed out by Winicour [25] with a conformal approach, whatever rescaling we take, the mass term always remains singular at $\mathscr{I}^+$. This can lead to numerical problems, such as blowup or a lack of convergence. One way of trying to tackle such issues is to derive special algorithms that respect physical restrictions, to make sure that errors are well behaved and that the code converges at the desired accuracy. One constraint of physical interest is provided by the energy conservation. If such a conserved energy is available, we can utilize it as an additional constraint on the dynamics of the field. In this subsection, we derive a conserved energy at the continuum level. Later, in Sec. IV, we will construct an approximation to this norm in our discretization.

1. Conserved energy with the original variables

Consider the functional $T_{\mu\nu}[\psi]$, with ψ satisfying the LWEP, given by

$$T_{\mu\nu} = \partial_\mu\psi\partial_\nu\psi - \frac{1}{2}g_{\mu\nu}(\partial^\alpha\psi\partial_\alpha\psi + F\psi^2), \tag{24}$$

which we will refer to as the stress-energy tensor. The time-independent potential F is non-negative for all R, bounded, and C^k for large k. In our setup, the stress-energy tensor is not necessarily covariantly conserved, but, for the purposes of this work, its utility comes down to the fact that it provides coercive estimates on solutions to the field equations. To see this, we follow the standard steps of the vector-field method. A clear introduction to this approach can be found in Ref. [34]. Consider a vector field K^μ and contract it with $T_{\mu\nu}$. Taking the total divergence and using the product rule, we get

$$\nabla^\mu(T_{\mu\nu}K^\nu) = (\nabla^\mu T_{\mu\nu})K^\nu + T_{\mu\nu}\nabla^\mu K^\nu. \tag{25}$$

Using Eq. (6) in the first term on the right-hand side, we obtain

$$\nabla^\mu(T_{\mu\nu}K^\nu) = -\frac{1}{2}K^\nu(\partial_\nu F)\psi^2 + T_{\mu\nu}\nabla^\mu K^\nu. \tag{26}$$

As shown in Fig. 2, consider a region $\mathcal{R}$ surrounded by a boundary ∂R consisting of the initial hyperboloidal slice Σ_0, some later hyperboloidal slice Σ_t, with $t > 0$, inner timelike constant radial boundary Σ_R, and future null infinity $\mathscr{I}^+$. Integrating Eq. (26) over $\mathcal{R}$ and applying Stokes' theorem on the left side of the equation yields

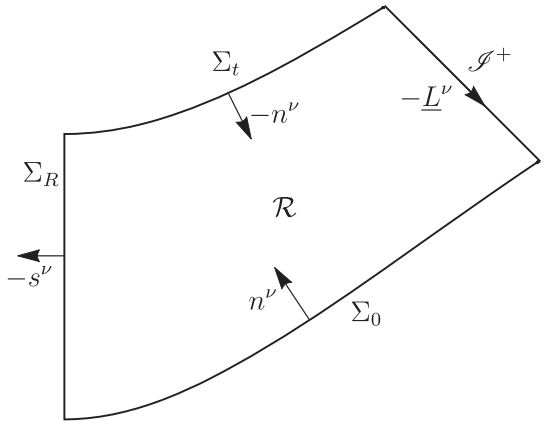

FIG. 2. Diagram depicting the spacetime region where Stokes' theorem is applied. The normal vectors follow the conventions of Ref. [34].

$$\int_{\Sigma_0} T_{\mu\nu}K^\mu n^\nu + \int_{\Sigma_t} T_{\mu\nu}K^\mu(-n^\nu) + \int_{\Sigma_R} T_{\mu\nu}K^\mu(-s^\nu) + \int_{\mathscr{I}^+} T_{\mu\nu}K^\mu(-\underline{L}^\nu) = \int_{\mathcal{R}}\left[T_{\mu\nu}\nabla^\mu K^\nu - \frac{1}{2}K^\nu(\partial_\nu F)\psi^2\right], \tag{27}$$

where $\underline{L}^\nu$ is the ingoing null vector at $\mathscr{I}^+$ as defined in Eq. (5) in Ref. [20] and s^ν is the spatial normal vector to Σ_R. The first term in the bulk integral on the right vanishes if K^μ is a Killing vector. Taking furthermore K^μ causal and recalling our restriction on the sign of the potential, it follows that the integrand on the two spatial slices Σ_0 and Σ_t is sign definite. If $K^\mu = (\partial_T)^\mu$, we get $K^\nu(\partial_\nu F) = \partial_T F = 0$, resulting in a vanishing bulk integral. Henceforth, we make this choice. Taking $R = 0$ at the inner boundary makes the Σ_R integral vanish. What remains is

$$\int_{\Sigma_0} T_{\mu\nu}K^\mu n^\nu - \int_{\Sigma_t} T_{\mu\nu}K^\mu n^\nu - \int_{\mathscr{I}^+} T_{\mu\nu}K^\mu\underline{L}^\nu = 0. \tag{28}$$

From the line element (4), we can compute

$$n^{\underline{\nu'}} = \alpha(1, 1 - 1/R', 0, 0), \qquad \underline{L}^{\underline{\nu}} = (\partial_T - \partial_R)^{\underline{\nu'}}. \tag{29}$$

Substituting these into Eq. (28), using Eq. (24), and moving now to work with our first-order reduction (using π and ϕ_R), we obtain

$$\left(\int_{\Sigma_t} - \int_{\Sigma_0}\right)\frac{\alpha}{2}\left[\pi^2 - 2\frac{R'-1}{R'}\pi\phi_R + \phi_R^2 + F\psi^2\right] = -\frac{1}{2}\int_{\mathscr{I}^+}[(\sigma^-)^2 + F\psi^2] \le 0. \tag{30}$$

The reduction admits the natural analog of Eq. (28) when $\gamma_2 = 0$, which we assume henceforth. Because $F \ge 0$ at $\mathscr{I}^+$, the right side of Eq. (30) is negative semidefinite. Thus, the energy on our hyperboloidal slices, given by the integrals on the left side, can leak out only through $\mathscr{I}^+$ and remains conserved only when the right side is identically zero. The flux of radiation through $\mathscr{I}^+$ will depend on the form of F, which plays a crucial role in the dynamics of the field. In all cases, the energy on the subsequent hyperboloidal slices is always upper bounded by the initial energy. Therefore, integrating out the trivial dependence on θ^A, the angular coordinates, we consider the energy norm

$$E(t) = \int_{\Sigma_t}\varepsilon dr. \tag{31}$$

Depending on our choice of variables, we write either

$$\varepsilon = \frac{1}{2}\left[\pi^2 - 2\left(\frac{R'-1}{R'}\right)\pi\phi_R + \phi_R^2 + F\psi^2\right]R^2R' \tag{32}$$

or

$$\varepsilon=\frac{1}{2}\left[\left(\frac{2R'-1}{2R'}\right)(\sigma^+)^2+\left(\frac{1}{2R'}\right)(\sigma^-)^2+F\psi^2\right]R^2R'. \quad (33)$$

Note the rather unusual convention, in which we are absorbing the volume form into the symmetrizer (the matrix that representing the quadratic form). Some care is needed to obtain the flux at infinity. Let us, thus, temporarily truncate the slices at an outer radius $r_o \le r_{\mathscr{J}}$ and take r_o to be some function of time t. We obtain then $E(t)=E(t,r_o(t))$ and

$$\frac{d}{dt}E(t,r_o)=\partial_t E(t,r_o)+\partial_{r_o}E(t,r_o)\cdot\left.\frac{dr_o}{dt}\right|_{r=r_o}. \quad (34)$$

Substitution from the equations of motion and integrating by parts gives for the first term

$$\partial_t E(t,r_o)=-R^2\phi_R\pi|_{r=r_o}=\left.\frac{1}{4}R^2[(\sigma^+)^2-(\sigma^-)^2]\right|_{r=r_o}, \quad (35)$$

while, from the definition of ε, we get

$$\partial_{r_o}E(t,r_o)=\lim_{\delta r_o\to 0}\frac{1}{\delta r_o}\left(\int_0^{r_o+\delta r_o}-\int_0^{r_o}\right)\varepsilon dr=\varepsilon(t,r_o). \quad (36)$$

If the outer boundary of the system is a timelike constant radius worldtube, then $dr_o/dt=0$, and the second term on the right of Eq. (34) vanishes. If, instead, it is an incoming null curve, so that $\dot{r}_o=dr_o/dt=c^r_-=-1/(2R'-1)$, we obtain

$$\begin{aligned}\frac{d}{dt}E(t,r_o)&=-\frac{1}{4}R^2\frac{2R'}{2R'-1}[F\psi^2+(\pi+\phi_R)^2]\Big|_{r=r_o}\\&=-\frac{1}{4}R^2\frac{2R'}{2R'-1}[F\psi^2+(\sigma^-)^2]\Big|_{r=r_o}.\end{aligned} \quad (37)$$

In the limit $r_o\to r_{\mathscr{J}}$, $2R'/(2R'-1)\to 1$, we recover

$$\begin{aligned}\frac{d}{dt}E(t,r_{\mathscr{J}})&=-\frac{1}{4}R^2[F\psi^2+(\pi+\phi_R)^2]\Big|_{r=r_{\mathscr{J}}}\\&=-\frac{1}{4}R^2[F\psi^2+(\sigma^-)^2]\Big|_{r=r_{\mathscr{J}}},\end{aligned} \quad (38)$$

consistent with the right side of Eq. (30)—note that a factor of $1/2$ appeared above because $\delta t=2\delta u$ there. In our case, we take $\dot{r}_o=c^r_-$, because $\mathscr{J}^+$ is incoming null. Note here that the right-hand side of this expression should still be understood in a limiting sense (as $r_o\to r_{\mathscr{J}}$). We will avoid this complication in the following by the use of rescaled variables. In deriving Eq. (38), the second term on the right-hand side of Eq. (34) is important. Since the hyperboloidal slices meet $\mathscr{J}^+$ rather than i^0, it appears naively that if we had just taken $\dot{r}_o=0$ and let $r_o\to r_{\mathscr{J}}$, we would still get the correct expression for dE/dt. Contrarily, as the foregoing discussion shows, this is not true.

2. Conserved energy with rescaled variables

In Eq. (38), as $r_o\to r_{\mathscr{J}}$, $R\to\infty$ and it becomes difficult to express dE/dt in closed form. But if we recall the rescaled variables (17),

$$\tilde{\psi}=\chi\psi,\qquad \tilde{\sigma}^+=\chi^2\sigma^+,\qquad \tilde{\sigma}^-=\chi\sigma^-, \quad (39)$$

where $\chi=\sqrt{1+R^2}$, all the coefficients in the above expressions in fact regularize except possibly the potential term. Examples that will be used later in the derivations are

$$\varepsilon=\frac{1}{2}\left[F\tilde{\psi}^2R'+\left(\frac{2R'-1}{2\chi^2}\right)(\tilde{\sigma}^+)^2+\frac{(\tilde{\sigma}^-)^2}{2}\right]\frac{R^2}{\chi^2} \quad (40)$$

for the energy density,

$$\begin{aligned}&\partial_{r_o}E(t,r_o(t))\cdot\frac{dr_o}{dt}\\&=-\frac{1}{2}\frac{1}{2R'-1}\cdot\left[F\tilde{\psi}^2R'+\left(\frac{2R'-1}{2\chi^2}\right)(\tilde{\sigma}^+)^2+\frac{(\tilde{\sigma}^-)^2}{2}\right]\frac{R^2}{\chi^2}\Big|_{r=r_o}\end{aligned} \quad (41)$$

for the moving-boundary term, and

$$\partial_t E(t,r_o)=\frac{1}{4}\left[\frac{\tilde{\sigma}^{+2}}{\chi^2}-\tilde{\sigma}^{-2}\right]\frac{R^2}{\chi^2}\Big|_{r=r_o} \quad (42)$$

for the remaining boundary term. In the limit $r_o=r_{\mathscr{J}}$, we have $R^2/\chi^2\to 1$ and, thus, get

$$\frac{d}{dt}E(t)=-\frac{1}{4}((\tilde{\sigma}^-)^2+F\tilde{\psi}^2)\Big|_{r=r_{\mathscr{J}}}. \quad (43)$$

The potential term in ε is, thus, still singular if F does not fall off fast enough. In that case, we still can choose initial data such that the product $R'F\psi^2$ is finite at $r_{\mathscr{J}}$. Using inequality (30), we can make sure that this whole term remains regular at $r_{\mathscr{J}}$ for all times t.

IV. SUMMATION BY PARTS SCHEME ON THE HYPERBOLOIDAL SLICES

Having laid out the continuum setup above, in this section we now present our discrete approximation. This involves the evolution equations, the conserved (up to boundary fluxes) energy, the use of regularized variables, and discrete operators satisfying SBP and TEM.

A. SBP and TEM overview

The energy estimate (43) shows that, for the continuum equations, the size of the solution at any time is bounded above by the size of the initial data plus an integral of the flux of radiation that leaves the domain through $\mathscr{I}^+$. The key idea of a summation by parts scheme is to discretize such a system so that the semidiscrete equations admit a similar estimate. Examples of the use of SBP schemes in numerical relativity include Refs. [35–39]. See the review in Ref. [40] for a more thorough discussion. We now give a brief summary of how that is achieved. Consider a first-order linear symmetric hyperbolic system for a state vector $\mathbf{u}$ with k components, each a scalar quantity on spacetime. The equation of motion is then written

$$\partial_t \mathbf{u} = \mathbf{A}^p(x^\mu)\partial_p \mathbf{u} + \mathbf{S}(x^\mu), \tag{44}$$

where x^ν are the spacetime coordinates. Here, p is summed over all spatial index values, and the principal part matrices $\mathbf{A}^p$ and source terms $\mathbf{S}(x^\mu)$ have the obvious dimensionality. We use boldface symbols to represent objects and operators with the dimensionality of the state vector. Symmetric hyperbolicity means that there exists a symmetrizer, a symmetric positive definite matrix $\mathbf{H}$, with the product $\mathbf{H}\mathbf{A}^p$ symmetric for each p.

In the context of numerical relativity, there is a natural concern that we restrict our attention to symmetric hyperbolic systems, since when coupled to the moving puncture gauge [41,42] popular formulations, such as BSSNOK by Baumgarte and Shapiro [43]; Shibata and Nakamura [44]; Nakamura, Oohara and Kojima [45] or Z4 by Bona *et al.* [46]; Bernuzzi *et al.* [47]; Alic *et al.* [48], may be strongly but not symmetric hyperbolic. Although the methods we develop may be applicable to these systems, demonstrating their efficacy rigorously would not be straightforward in 3D. Nevertheless, in our approach [17] we are primarily focused on the use of a first-order reduction of GR in generalized harmonic gauge, which is indeed symmetric hyperbolic.

Suppose that we solve the initial boundary value problem for our system on a compact spatial domain $V(t)$ with boundary $\partial V(t)$. Then we have the energy

$$E(t) = \int_{V(t)} \frac{1}{2}\mathbf{u}^T\mathbf{H}\mathbf{u}, \tag{45}$$

where the superscript T denotes the matrix transpose. This energy norm satisfies

$$\frac{d}{dt}E(t) = \int_{\partial V(t)} \frac{1}{2}\mathbf{u}^T\mathbf{H}(\mathbf{A}^p s_p + v^p s_p \mathbf{1})\mathbf{u} + \text{bulk term}, \tag{46}$$

where the bulk term, an integral over $V(t)$, can, in general, be seen to be bounded using a combination of the Grönwall and Cauchy-Schwarz inequalities, $v^p = \partial_t x^p(t)$ denotes the local velocity of the outer boundary, and s_p denotes the outward-pointing unit normal to the domain at the boundary. We assume, as in our hyperboloidal setup, that the bulk term vanishes and that the boundary integral is nonpositive. Now discretize the equations first by introducing the spatial grid x^p_I, with index I labeling the grid points. We replace the continuum state vector $\mathbf{u}$ by a discrete analog $\mathbf{U}$ that lives on the grid and, thus, has components U^α_I for each continuum field, with α here labeling the different continuum fields. We need an approximation to the spatial derivative ∂_p, which we denote here as D_i. In our specific setup, this last step is more subtle, because, following Refs. [31–33], the use of shell coordinates (spherical polars) requires us to introduce two different approximations. But to illustrate the general approach we sweep nonessential complications under the carpet at this stage. We work with the semidiscrete approximation, writing the large collection of ordinary differential equations for the components of $\mathbf{U}$ as

$$\frac{d}{dt}\mathbf{U} = \mathbf{A}^p(t, x_I)D_p\mathbf{U} + \mathbf{S}(t, x_I). \tag{47}$$

At this point, different options are available, and we will choose the simplest. See Ref. [37] for a discussion of the alternatives. Consider now the discrete approximation to Eq. (44), given by the sum over grid points

$$E(t) = \frac{1}{2}(\mathbf{U}, \mathbf{U})_{\mathbf{H}} \equiv \frac{1}{2}\sum_I \mathbf{U}^T_I \Upsilon_I \mathbf{H}_I \mathbf{U}_I, \tag{48}$$

where $\mathbf{H}_I = \mathbf{H}(t, x_I)$ and $\Upsilon_I \equiv \Upsilon_I \mathbf{1}$, which we call the quadrature or quadrature matrix ($\mathbf{1}$ here is the $k \times k$ identity matrix associated with the state space) encodes information about the local grid spacing at point I. For simplicity, the norm is taken to be diagonal over grid points. Computing the time derivative, we get

$$\frac{d}{dt}(2E(t)) = (\mathbf{A}^p D_p\mathbf{U}, \mathbf{U})_{\mathbf{H}} + (\mathbf{U}, \mathbf{A}^p D_p\mathbf{U})_{\mathbf{H}} + ((\ln\Upsilon)^{\cdot}\mathbf{U}, \mathbf{U})_{\mathbf{H}} + \text{bulk term}, \tag{49}$$

with the shorthand $((\ln\Upsilon)^{\cdot}\mathbf{U})_I = (d/dt(\ln\Upsilon_I))\mathbf{U}_I$. Now observe that the discretization can be carefully chosen so that

$$(\mathbf{A}^p D_p\mathbf{U}, \mathbf{U})_{\mathbf{H}} + (\mathbf{U}, \mathbf{A}^p D_p\mathbf{U})_{\mathbf{H}} + ((\ln\Upsilon)^{\cdot}\mathbf{U}, \mathbf{U})_{\mathbf{H}} = (\mathbf{U}, (\mathbf{A}^p s_p + \mathbf{1}v^p s_p)\mathbf{U})_{\mathbf{H},\partial V} + \text{bulk term}, \tag{50}$$

where it must be possible to bound the bulk term by $E(t)$ multiplied by a constant that is independent of resolution, encoded in our notation by Υ_I, times $E(t)$. Here we have defined a boundary inner product and associated norm,

$$(\mathbf{U}, \mathbf{V})_{\mathbf{H},\partial V} = \sum_B \mathbf{U}^T_B \Upsilon_B \mathbf{H}_B \mathbf{V}_B, \tag{51}$$

with the sum here taken over the set of boundary points, denoted throughout by an index B. We may then conclude that the continuum energy conservation equation (46) has the semidiscrete analog

$$\frac{d}{dt}E(t) = (\mathbf{U}, (\mathbf{A}^p s_p + \mathbf{1}v^p s_p)\mathbf{U})_{\mathbf{H},\partial V} + \text{bulk term}. \quad (52)$$

If a condition like Eq. (50) is satisfied, the method is called a summation by parts scheme. Such a scheme has the advantage that, under mild assumptions on the coefficient matrices and source terms and the use of suitable boundary conditions, solutions of the approximation are guaranteed to converge to solutions of the continuum system in the limit of infinite resolution [49]. The specific rate of convergence is determined by the choice of approximation to the spatial derivative. In numerical relativity, the two most popular choices are to use a spectral approximation or finite differences.

Despite its strengths, naively applying the SBP approach may result in a scheme with undesirable features. For example, insisting that the semidiscrete and continuum energies match exactly, say, by careful adjustment of the derivative operators near the boundary, can result in the creation of numerical noise that propagates into the domain. In the hyperboloidal setting, we might already suspect that such noise would be problematic, since everything about our coordinates is engineered with the resolution of outgoing rather than incoming waves in mind. One might counter that, since the method would be guaranteed to converge in some norm, we could just increase the resolution to suppress the noise, but several points stand against this perspective. The final aim of our research program is to provide gravitational waveforms at null infinity. Since these waveforms will be used for modeling, they should be as clean as possible *pointwise* even at finite resolution. In other words, the natural mathematical measure of error provided by the problem may not correspond with the notion of error required of the data in applications. Second, the norm that the equations naturally provide (40), in fact, degenerates in the incoming characteristic variable $\tilde{\sigma}^+$, in that the coefficient multiplying that variable goes to zero near $\mathscr{I}^+$, if the compactification parameter $n < 2$. In some of the models in this paper, we could choose $n = 2$. However, owing to the presence of log terms in the natural expansion near $\mathscr{I}^+$ in our gauge, no formulation is presently available for GR in which $n = 2$ is permissible under our approach. Observe in passing that this degeneracy appears also on null slices even for the wave equation and so is not surprising. We aim, therefore, here to develop a method that satisfies semidiscrete estimates like Eq. (40) but which minimizes dangerous reflections from the outer boundary.

To that end let us illustrate, as summarized nicely in Ref. [24], the utility of TEM by considering two finite-difference approximations to the first derivative. Suppose that in the bulk domain we have a one-dimensional uniform grid with spacing h and the approximation

$$DF_I = \frac{1}{2h}(F_{I+1} - F_{I-1}), \quad (53)$$

to the first derivative using the arbitrary grid function F, which should not be confused with the potential, but that at the outer boundary $I = N$ we take one of

$$DF_N = \frac{1}{2h}(3F_N - 4F_{N-1} + F_{N-2}),$$
$$DF_N = \frac{1}{2h}(4F_N - 7F_{N-1} + 4F_{N-2} - F_{N-3}). \quad (54)$$

Either choice results in a second-order accurate approximation to the first derivative. Assuming we are approximating with F a C^3 continuum function f, we can Taylor expand and find, using the standard little-oh notation, that the error coefficient takes the form

$$DF_I = f'(x_I) + \frac{1}{6}h^2 f'''(x_I) + o(h^2), \qquad I < N,$$
$$DF_N = f'(x_I) - \frac{1}{3}h^2 f'''(x_I) + o(h^2), \qquad I = N \quad (55)$$

in the first case and

$$DF_I = f'(x_I) + \frac{1}{6}h^2 f'''(x_I) + o(h^2) \quad (56)$$

everywhere in the second. In the first case, the coefficient in front of the h^2 error term is different, which will induce (convergent) high-frequency noise, whereas in the second the approximation was carefully chosen at the boundary so that the errors match up. In what follows, we exploit this, the basic idea of TEM, to minimize high-frequency reflections from $\mathscr{I}^+$.

B. Discretization

All our derivations will be done for a nonstaggered grid, which includes a grid point at the boundaries. Let the radial coordinate r take discrete values $\{r_0, \ldots, r_N\}$. We take a uniform grid with step size h, which gives

$$r_I = Ih, \quad \text{with } I = 0, \ldots, N, \quad (57)$$

where N is a positive integer. Here, N corresponds to the grid index at the outer boundary. Although the origin is not a physical boundary point, it is convenient to treat it as a boundary while defining the grid on the closed interval $[0, r_o]$ and give boundary conditions in terms of the parity of the various fields. As before, r_o corresponds to the compactified radial coordinate at the outer boundary.

We will define our discretization using a single grid variable ψ instead of the whole state vector $\mathbf{u}$, since the basic idea remains the same. Define $\Psi_I(t) = \psi(t, r_I)$, assuming that $\psi(t, r)$ is a sufficiently smooth function of r, and, for convenience, we drop the argument t. Let Ψ to be

the column vector with Ψ_I as its Ith element. We express every linear operator, e.g., the finite-difference operator D, acting on Ψ as an $(N+1)\times(N+1)$ matrix. While writing the discrete form of the continuum equations, we express various coefficients that appear, which are, in general, functions of r, as $(N+1)\times(N+1)$ matrices. This step will become clearer in the next subsection. In the next paragraph, we describe the general notation and properties of these multiplication operators.

We denote the operators in the approximation corresponding to various coefficient functions of r in the equations of motion by writing their continuum names in square brackets. For example, we denote by $[f(r)]$ the operator, or $(N+1)\times(N+1)$ matrix, corresponding to the function $f(r)$ in the continuum limit. For simplicity, we take these matrices to be diagonal with diagonal entries $[f(r)]_{II} = f(r_I)$. Being diagonal, all these operators satisfy the same basic algebraic properties, such as commutativity, as the corresponding continuum functions.

We define all our discrete norms using a centered grid, in which each interval, of size h, in the bulk is taken symmetrically about its respective grid point. Therefore, the boundary points are left with the intervals of size $h/2$ which lie only toward the bulk, so that the sum of intervals remains Nh. If the state vector $\mathbf{U}$ contains only a single variable $U^1 = \Psi$, the quadrature reduces to a 1×1 matrix in the state space, $\Upsilon = [\Upsilon]$. Here, Υ is a scalar in the state space but an $(N+1)\times(N+1)$ matrix in the grid space. For simplicity, we take it to be a diagonal matrix:

$$\Upsilon = \mathrm{diag}(h/2, h, \ldots, h, h/2). \tag{58}$$

The same arguments apply to the symmetrizer as well, which takes the form $\mathbf{H} = [W]$, where W is just a scalar in the state space and an $(N+1)\times(N+1)$ diagonal matrix in the grid space:

$$W = \mathrm{diag}(w_0, \ldots, w_N). \tag{59}$$

These conventions lead to the following definition for the norm of a single grid function Ψ:

$$\|\Psi\|_{\mathbf{H}} = \Psi^T \Upsilon W \Psi. \tag{60}$$

Assuming W is time independent, the only time dependence appears in Ψ.

In our system, we will face the situation in which the coordinate position of the outer boundary is a continuous function of time. To realize this in our numerics, we keep our grid uniform in the bulk, with width $= h$, but make the position of the last grid point a continuous function of time, so that it moves with the outer boundary. However, we impose that the maximum value the last grid width can take is h. If the outer boundary moves further, we create a new, $(N+1)$th grid point, at r_N at that instant which moves with the outer boundary. If, let us say at time t_1, the outer boundary reaches a distance h away from r_N and still keeps moving outward, this $(N+1)$th grid point gets fixed there and a newer, $(N+2)$th grid point is created at $r_{N+1} = (N+1)h$ at that instant, and so on. We can model the reverse situation, in which the outer boundary moves inward, in exactly the reverse way. That is, when the last grid point merges with the penultimate one, it vanishes and the penultimate one becomes the last grid point, and so on.

The next problem is to incorporate the moving outer boundary in the definition of the norm. As before, we keep the elements of W time independent but make its dimensionality a function of time. The latter condition also applies to the quadrature Υ, but we make its last entry a function of time by redefining it as

$$\Upsilon = \mathrm{diag}(h_0, \ldots, h_N), \tag{61}$$

with $h_0 = h/2$ and $h_I = h$ for $I = 1, \ldots, N-1$. Here, h_N can take only values in $0 < h_N \leq h$. Its relationship with the creation or annihilation of the last grid point is "out of phase" as follows. Whenever $(r_N - r_{N-1}) > h/2$, Υ is given by Eq. (61) with h_N given by

$$h_N = r_N - r_{N-1} - \frac{h}{2} \tag{62}$$

and the norm is given by Eq. (60). However, when $(r_N - r_{N-1}) \leq h/2$, we do not consider the contribution of the last grid point to the norm, which is the same as removing the last row of Ψ, W, and Υ and the last column of W and Υ in Eq. (60), with Υ as given by Eq. (61). In this case, the effect of the moving boundary is captured by h_{N-1}, and its value is given by

$$h_{N-1} = r_N - r_{N-1} + \frac{h}{2} \quad \text{for } 0 \leq r_N - r_{N-1} \leq \frac{h}{2}. \tag{63}$$

In summary, for the case of a moving outer boundary, we define the discrete norm by Eq. (60), taking $\Psi = (\Psi_0, \ldots, \Psi_M)^T$, $W = \mathrm{diag}(w_0, \ldots, w_M)$, and $\Upsilon = \mathrm{diag}(h_0, \ldots, h_M)$, with $h_0 = h/2$, $h_i = h$ for $i = 1, \ldots, M-1$. We take $M = N$ whenever $(r_N - r_{N-1}) > h/2$, in which case h_N is given by Eq. (62), and $M = N-1$ whenever $(r_N - r_{N-1}) \leq h/2$, with h_{N-1} given by Eq. (63). On the initial slice, we set $h_N = h/2$.

Therefore, the total time derivative of the norm becomes

$$\frac{d}{dt}\|\Psi\|_{\mathbf{H}} = 2\Psi^T \Upsilon W \dot{\Psi} + \Psi^T \dot{\Upsilon} W \Psi, \tag{64}$$

where $\dot{\Psi} = d\Psi/dt$ and $\dot{\Upsilon} = d\Upsilon/dt$. The second term appears solely because of the moving outer boundary. Using the chain rule, we get

$$\dot{\Upsilon} = \frac{\partial \Upsilon}{\partial r_N} \dot{r}_N. \tag{65}$$

Substituting the definitions given in the previous paragraph along with Eqs. (62) and (63), we obtain

$$\Psi^T \dot{\Upsilon} W \Psi = w_M \Psi_M^2 \dot{r}_N, \tag{66}$$

with $M = N$ for $(r_N - r_{N-1}) > h/2$ and $M = N-1$ for $(r_N - r_{N-1}) \leq h/2$. When the trajectory of r_N is of an incoming radial null ray, we get

$$\dot{r}_N = c_-^r|_{r=r_N} = -\frac{1}{2R'_N - 1}, \tag{67}$$

where $R'_N = R'(r_N)$. Therefore, when the outer boundary is at $r_{\mathscr{I}}$, this gives $\Psi^T \dot{\Upsilon} W \Psi = 0$.

All these computations are easily generalized to a state vector $\mathbf{U}$ belonging to the higher-dimensional state space by working in a basis which diagonalize $\mathbf{H}$ and Υ in that space. Since the quadrature Υ depends only on the grid spacing and not on the dynamical variables, it should be a scalar multiple of the identity matrix acting on the state space. In that case, we can write

$$\mathbf{H} = \mathrm{diag}(W_1, \ldots, W_k), \tag{68}$$

where, as introduced in Eq. (44), k is the dimension of the state space.

C. $(\psi, \sigma^+, \sigma^-)$ system

In the next two subsections, we now discretize the $(\psi, \sigma^+, \sigma^-)$ system of equations (11) and define a semidiscrete energy. Demanding conservation of this discrete energy up to a boundary term in the usual way, we obtain our SBP scheme. Whenever working with the semidiscrete setting, we set the constraint damping parameter $\gamma_2 = 0$. This has the advantage of simplifying the energy estimates by rendering the bulk term trivial, and, at least in the linear setting, we shall see has no negative consequences for constraint violation. The latter may need revisiting when we tackle nonlinear problems like GR but, since we are developing a scheme with the linear-dominated wave zone in mind, seems reasonable. Following the conventions of Sec. IV B, we define $\Psi_I(t) \coloneqq \psi(t, r_I)$, $\Sigma_I^+(t) \coloneqq \sigma^+(t, r_I)$, and $\Sigma_I^-(t) \coloneqq \sigma^-(t, r_I)$ and suppress the t dependence. Define the column vectors Ψ, Σ^+, and Σ^- with Ith entries as Ψ_I, Σ_I^+, and Σ_I^-, respectively. The state vector for our system is then $\mathbf{U} = (\Psi, \Sigma^+, \Sigma^-)^T$.

Let D and $\bar{D}$ denote the finite-difference operators represented by $(N+1) \times (N+1)$ matrices such that $\Upsilon^{-1} D$ and $\Upsilon^{-1} \bar{D}$ approximate ∂_r and $\partial_r + 2R'/R$, respectively, at the discrete level. Here, Υ is the same quadrature matrix defined in Eq. (61). Therefore, motivated from Eq. (11), we define our finite-difference scheme as

$$\begin{aligned}
\dot{\Psi} &= \frac{\Sigma^+ + \Sigma^-}{2}, \\
\dot{\Sigma}^+ &= \left[\frac{1}{2R'-1}\right] \Upsilon^{-1} \left(\frac{(D+\bar{D})}{2} \Sigma^+ + \frac{(D-\bar{D})}{2} \Sigma^- \right) \\
&\quad - \left[\frac{R'}{2R'-1}\right] [F] \Psi, \\
\dot{\Sigma}^- &= -\Upsilon^{-1} \left(\frac{(D+\bar{D})}{2} \Sigma^- + \frac{(D-\bar{D})}{2} \Sigma^+ \right) - [R'][F]\Psi.
\end{aligned} \tag{69}$$

As introduced in the previous section, the quantities in square brackets denote the discrete operators corresponding to the continuum functions written inside them. This makes sense because R' and F are functions of r.

Motivated by Eqs. (31) and (33), we define our discrete energy norm as

$$\hat{E} = \frac{1}{2} (\Psi^T [F] \Upsilon W \Psi + (\Sigma^+)^T \Upsilon W^+ \Sigma^+ + (\Sigma^-)^T \Upsilon W^- \Sigma^-). \tag{70}$$

Here, the various W's are the $(N+1) \times (N+1)$ weight matrices just like W in the last subsection. Therefore, the symmetrizer matrix here is the diagonal matrix with blocks $\mathbf{H} = \mathrm{diag}(W, W^+, W^-)$. So far, we demand only that the matrices W, W^+, and W^- are positive and diagonal.

The discrete energy defined above is a function of time and the outer boundary r_N, which again is a function of time, i.e., $\hat{E} = \hat{E}(t, r_N(t))$. The contribution to change in energy solely from the evolved variables is

$$\partial_t \hat{E} = [\Psi^T [F] \Upsilon W \dot{\Psi} + (\Sigma^+)^T \Upsilon W^+ \dot{\Sigma}^+ + (\Sigma^-)^T \Upsilon W^- \dot{\Sigma}^-]. \tag{71}$$

Substituting the evolution equations (69) and using various algebraic relations and symmetry properties, we obtain

$$\begin{aligned}
\partial_t \hat{E} = &\left[(\Sigma^+)^T \frac{\Upsilon}{2} \left(W - W^+ \left[\frac{2R'}{2R'-1}\right] \right) + (\Sigma^-)^T \frac{\Upsilon}{2} \right. \\
&\left. \times (W - W^-[2R']) \right] [F] \Psi + \left[(\Sigma^+)^T W^+ \left[\frac{1}{2R'-1}\right] \right. \\
&\left. \times \left(\frac{D+\bar{D}}{2}\right) \Sigma^+ - (\Sigma^-)^T W^- \left(\frac{D+\bar{D}}{2}\right) \Sigma^- \right] \\
&+ \left[(\Sigma^+)^T W^+ \left[\frac{1}{2R'-1}\right] \left(\frac{D-\bar{D}}{2}\right) \Sigma^- \right. \\
&\left. - (\Sigma^-)^T W^- \left(\frac{D-\bar{D}}{2}\right) \Sigma^+ \right].
\end{aligned} \tag{72}$$

In order to derive an SBP scheme, this energy is required to be conserved up to the boundary term, which was not

imposed up to this point. Hence, motivated by the continuum expression (35), we demand

$$\partial_t \hat{E} = (\Sigma^+)^T B \Sigma^+ - (\Sigma^-)^T B \Sigma^-, \tag{73}$$

which gives first

$$W = W^+\left[\frac{2R'}{2R'-1}\right] = W^-[2R'], \tag{74}$$

then

$$W^-\left(\frac{D+\bar{D}}{2}\right) = B, \tag{75}$$

and finally

$$W^-\left(\frac{D-\bar{D}}{2}\right) - \left(W^-\left(\frac{D-\bar{D}}{2}\right)\right)^T = 0. \tag{76}$$

This gives our SBP scheme

$$W^-\bar{D} + D^T W^- = B + B^T \tag{77}$$

or, isolating instead $\bar{D}$,

$$\bar{D} = -(W^-)^{-1} D^T W^- + (W^-)^{-1}(B + B^T). \tag{78}$$

Here, B is called the boundary matrix or boundary operator. As the name suggests, this matrix is expected to be nonzero only at (or near) the outer boundary. These relations are analogous to those given in the continuum energy norm (40), which is already promising.

We take the outer boundary to be an incoming null ray at a finite coordinate radius r_N. Using the same argument as in Eqs. (64) and (66) and using Eq. (67), the effect of the moving outer boundary to the change in energy is

$$\begin{aligned}(\partial_{r_N}\hat{E})\dot{r}_N &= -\frac{1}{2}[F_N w_N \Psi_N^2 + w_N^+(\Sigma_N^+)^2 + w_N^-(\Sigma_N^-)^2] \\ &\quad\cdot\frac{1}{2R'_N-1} \\ &= -\frac{1}{2}w_N^-\left[F_N\frac{2R'_N}{2R'_N-1}\Psi_N^2 + (\Sigma_N^+)^2 \right. \\ &\quad \left. + \frac{1}{2R'_N-1}(\Sigma_N^-)^2\right],\end{aligned} \tag{79}$$

where we use the obvious generalization of the notation (59) for $W^\pm$ and the relations (74). Unlike in the last subsection, we do not need to use the index M instead of N here because, as $r_N \to r_{\mathscr{I}}$, $\dot{r}_N \to 0$. Therefore, the total change in energy becomes

$$\begin{aligned}\dot{\hat{E}} &= \frac{d}{dt}\hat{E} = \partial_t \hat{E} + (\partial_{r_N}\hat{E})\dot{r}_N \\ &= -\frac{1}{2}w_N^- F_N \frac{2R'_N}{2R'_N-1}\Psi_N^2 - \frac{1}{2}w_N^-(\Sigma_N^+)^2 + (\Sigma^+)^T B\Sigma^+ \\ &\quad -\frac{1}{2}w_N^-\frac{1}{2R'_N-1}(\Sigma_N^-)^2 - (\Sigma^-)^T B\Sigma^-.\end{aligned} \tag{80}$$

The SBP relation (77), or, equivalently, (78), dictates the way in which the four operators D, $\bar{D}$, U^-, and B should be related. Therefore, given three of them, it can be used to derive the fourth one. We will choose D and B by hand and describe a method to choose U^- and, hence, derive $\bar{D}$. We define our methods with a second-order accurate operator D given by

$$(D\Psi)_I = \frac{\Psi_{I+1} - \Psi_{I-1}}{2} \tag{81}$$

in the bulk. A similar method can be applied for any higher-order accurate operator D as well. Choosing

$$B = \mathrm{diag}(0, \ldots, 0, B_N), \tag{82}$$

the SBP relation (78) gives

$$(\bar{D}\Psi)_I = -(W^{-1}D^T W\Psi)_I = \frac{w_{I+1}\Psi_{I+1} - w_{I-1}\Psi_{I-1}}{2w_I} \tag{83}$$

in the bulk. We use two methods described in Ref. [50]. One method is by Evans, given in Ref. [31] and described as follows. The continuum identity

$$\partial_r\psi + \frac{2R'}{R}\psi = 3R'\frac{d(R^2\psi)/dr}{d(R^3)/dr} \tag{84}$$

suggests one form for $\bar{D}$. To keep it consistent with Eq. (83), we define

$$(\bar{D}\Psi)_I = \frac{\frac{(R^3_{I+2}-R^3_I)}{12hR'_{I+1}}\Psi_{I+1} - \frac{(R^3_I - R^3_{I-2})}{12hR'_{I-1}}\Psi_{I-1}}{2\frac{(R^3_{I+1}-R^3_{I-1})}{12hR'_I}} \tag{85}$$

in the bulk. This suggests to us the choice $w_I^- = (R^3_{I+1} - R^3_{I-1})/12hR'_I$ for all I, which reduces to $R^2/2$ in the continuum limit. This extra half factor makes the discrete energy norm compatible with the continuum one.

The other method is described in Refs. [33,36] and uses the identity

$$\partial_r\psi + \frac{2R'}{R}\psi = \frac{\partial_r(R^2\psi)}{R^2}. \tag{86}$$

This suggests $w_I^- = R_I^2/2$ for all I. Following the terminology of Ref. [50], we refer to this as the Sarbach method.

Note that it is simpler to define w_I^- using this method at larger radii than Evans' method, but Evans' method is more convenient near $r = 0$, since it avoids the singular form of $1/R$ at the origin.

D. Regularization scheme

We know from the previous section that $R_N \to \infty$ as $r_N \to r_{\mathscr{I}}$, making B, w_N^-, and, hence, $\bar{D}$ singular at $r_{\mathscr{I}}$. Although this singular nature of $\bar{D}$ is expected due to the singular nature of R'/R at $\mathscr{I}^+$, it becomes impossible to define it at $r_{\mathscr{I}}$. To avoid this, we need to regularize $\bar{D}$ as well. In this section, we therefore study the regularization scheme of $\bar{D}$ obtained with Sarbach's method, which is simple and naturally allows us to set the outer boundary at $\mathscr{I}^+$. The regularization is not only "nice" but also necessary to straightforwardly apply results, such as the Lax equivalence theorem, from numerical analysis; see, for example, Ref. [49] for details. This is because the formal definition of numerical stability requires arbitrary given data with a finite norm to be admissible, which will not be the case if there are singular coefficients in the problem. Similar issues arise when treating the origin in spherical polar coordinates, but unfortunately at infinity we cannot rely on parity to help.

1. Regularized $\bar{D}$

We define a new operator $\tilde{D}$ by

$$\tilde{D} = P^{-2}\bar{D}P^2 \tag{87}$$

in such a way that all the entries of the matrix $\tilde{D}$ are $O(1)$ in the interval $[0, r_{\mathscr{I}}]$. Since, using Sarbach's method, the coefficients in $\bar{D}$ blow up like R^2 at $\mathscr{I}^+$, the entries of P should fall off like R^{-1}. We take P to be an $(N+1)\times(N+1)$ diagonal matrix with diagonal elements

$$P_{II} = \frac{1}{\sqrt{1+R_{II}^2}} = \frac{1}{\chi_I} \quad \text{for } I = 0, \ldots, N. \tag{88}$$

We choose $1 + R^2$, instead of R^2, simply to avoid singularities at the origin. With this definition, the singular part of $\bar{D}$ at $\mathscr{I}^+$ is absorbed by the matrices P^2 and P^{-2}.

Since, in the continuum limit, $P(r) = 1/\chi$, where $\chi^2 = 1 + R^2$ as defined previously, one can check that this choice of $\tilde{D}$ corresponds to the operator defined in Eq. (19) [equivalently, Eq. (20)] as

$$\tilde{D} \to \chi^2\left(\partial_r + \frac{2R'}{R}\right)\chi^{-2} = \partial_r + \frac{2R'}{(1+R^2)R} = \tilde{\partial}_r, \tag{89}$$

thus justifying the definition.

2. Regularized variables and operators

Naively, one might expect that, writing a discrete version of Eqs. (22) and defining $\tilde{W}^- = P^T W^- P$ and $\tilde{B} = P^T B P$, one obtains the SBP scheme with

$$\tilde{D} = -(\tilde{W}^-)^{-1}D^T\tilde{W}^- + (\tilde{W}^-)^{-1}(\tilde{B} + \tilde{B}^T) \tag{90}$$

for the regular equations. But this turns out not to be the case, because the additional rescaling of σ^+ by a factor of χ, compared to the other variables, does not play any role in the definition of $\tilde{D}$. This is also evident from Eq. (42), as we want the same boundary matrix acting on all of the dynamical variables. Therefore, to derive an SBP scheme for the regular equations with the most aggressively rescaled variables, we first rescale all the dynamical variables by a single power of χ, derive equations of motion, and *then* replace $\bar{\sigma}^+(\equiv\chi\sigma^+)$ by $(\tilde{\sigma}^+/\chi)$. This reduces Eqs. (22) to the following form:

$$\begin{aligned}
\partial_t\tilde{\psi} &= \frac{1}{2}\left[\frac{\tilde{\sigma}^+}{\chi} + \tilde{\sigma}^-\right],\\
\partial_t\tilde{\sigma}^+ &= \frac{1}{2R'-1}\left[\chi\left(\frac{\partial_r+\tilde{\partial}_r}{2}\right)\left(\frac{\tilde{\sigma}^+}{\chi}\right) + \chi\left(\frac{\partial_r-\tilde{\partial}_r}{2}\right)\tilde{\sigma}^-\right.\\
&\quad \left. - \frac{RR'}{\chi}\tilde{\sigma}^- - R'\chi F\tilde{\psi}\right] + \gamma_2\left[\frac{1}{2R'-1}\left(\chi(\partial_r\tilde{\psi})\right.\right.\\
&\quad \left.\left. - \frac{R}{\chi}R'\tilde{\psi} + \chi\frac{\tilde{\sigma}^-}{2}\right) - \frac{\tilde{\sigma}^+}{2}\right],\\
\partial_t\tilde{\sigma}^- &= -\left[\left(\frac{\partial_r+\tilde{\partial}_r}{2}\right)\tilde{\sigma}^- + \left(\frac{\partial_r-\tilde{\partial}_r}{2}\right)\left(\frac{\tilde{\sigma}^+}{\chi}\right)\right.\\
&\quad \left. - \frac{RR'}{\chi^3}\tilde{\sigma}^+ + R'F\tilde{\psi}\right] - \gamma_2\left[\partial_r\tilde{\psi} - \frac{R}{\chi^2}R'\tilde{\psi}\right.\\
&\quad \left. + \frac{\tilde{\sigma}^-}{2} - (2R'-1)\frac{\tilde{\sigma}^+}{2\chi}\right].
\end{aligned} \tag{91}$$

The semidiscrete form, with $\gamma_2 = 0$, is

$$\begin{aligned}
\dot{\tilde{\Psi}} &= \frac{1}{2}[P\tilde{\Sigma}^+ + \tilde{\Sigma}^-],\\
\dot{\tilde{\Sigma}}^+ &= \left[\frac{1}{2R'-1}\right]\left[P^{-1}\Upsilon^{-1}\left(\frac{D+\tilde{D}}{2}\right)P\tilde{\Sigma}^+ + P^{-1}\Upsilon^{-1}\right.\\
&\quad \left.\times\left(\frac{D-\tilde{D}}{2}\right)\tilde{\Sigma}^- - P[RR']\tilde{\Sigma}^- - P^{-1}[R'][F]\tilde{\Psi}\right],\\
\dot{\tilde{\Sigma}}^- &= -\left[\Upsilon^{-1}\left(\frac{D+\tilde{D}}{2}\right)\tilde{\Sigma}^- + \Upsilon^{-1}\left(\frac{D-\tilde{D}}{2}\right)P\tilde{\Sigma}^+\right.\\
&\quad \left. - P^2[RR']P\tilde{\Sigma}^+ + [R'][F]\tilde{\Psi}\right].
\end{aligned} \tag{92}$$

Defining the discrete energy as

$$\hat{E} = \frac{1}{2}[\tilde{\Psi}^T[F]\Upsilon\tilde{W}\tilde{\Psi} + (\tilde{\Sigma}^+)^T\Upsilon\tilde{W}^+\tilde{\Sigma}^+ + (\tilde{\Sigma}^-)^T\Upsilon\tilde{W}^-\tilde{\Sigma}^-] \tag{93}$$

and following the same procedure as above, we demand

$$\partial_t \hat{E} = (\tilde{\Sigma}^+)^T P^T \tilde{B} P \tilde{\Sigma}^+ - (\tilde{\Sigma}^-)^T \tilde{B} \tilde{\Sigma}^-, \tag{94}$$

which gives

$$\tilde{W} = P^{-2}\tilde{W}^+\left[\frac{2R'}{2R'-1}\right] = \tilde{W}^-[2R'], \tag{95}$$

$$\tilde{W}^-\left(\frac{D+\tilde{D}}{2}\right) = \tilde{B}, \tag{96}$$

and

$$\tilde{W}^-\left(\frac{D-\tilde{D}}{2}\right) - \left(\tilde{W}^-\left(\frac{D-\tilde{D}}{2}\right)\right)^T = 0. \tag{97}$$

This leads to the SBP scheme given by Eq. (90). Equations (92) are the ones used in the code. Provided the potential function F falls off fast enough, they are formally regular and satisfy the SBP property.

3. Constraints

The reduction constraint $C = \partial_R \psi - \phi_R$, written in terms of the rescaled fields $(\tilde{\psi}, \tilde{\sigma}^+, \tilde{\sigma}^-)$ and using a suitable rescaling, takes the form

$$\begin{aligned}\mathcal{C} &= \frac{R'\chi}{2R'-1}C \\ &= \frac{1}{2R'-1}\left(\partial_r\tilde{\psi} - \frac{RR'}{\chi^2}\tilde{\psi} + \frac{\tilde{\sigma}^-}{2}\right) - \frac{\tilde{\sigma}^+}{2\chi}.\end{aligned} \tag{98}$$

It also appears as the coefficient of $\gamma_2\chi$ in the second equation of Eqs. (18). In the continuum case, if the constraint is satisfied by the initial data, it will remain satisfied in the time development. However, this might not be the case at the discrete level. Defining the discrete form of Eq. (98) as

$$\hat{\mathcal{C}} = \left[\frac{1}{2R'-1}\right]\left(\Upsilon^{-1}D\tilde{\Psi} - P^2[RR']\tilde{\Psi} + \frac{\tilde{\Sigma}^-}{2}\right) - \frac{P}{2}\tilde{\Sigma}^+, \tag{99}$$

taking the time derivative, and substituting the equations of motion (92), we obtain $\dot{\hat{\mathcal{C}}} = 0$. Therefore, in our discretization scheme as well, if the constraint is satisfied on the initial data, it will remain satisfied forever. Thus, taking $\gamma_2 = 0$ in our discretization scheme is perfectly justified. But, in general, this will not necessarily be the case for a system of nonlinear equations.

E. Truncation error matching

Taking $\Upsilon = \mathrm{diag}(h/2, h, \ldots, h, h/2)$, the operator D defined with second-order accuracy by Eq. (81) in the bulk has the Taylor expansion

$$(Df)_I = h\left[f'_I + \frac{h^2}{6}f'''_I + \cdots\right], \qquad I = 0, \ldots, N-1. \tag{100}$$

Incorporating the TEM property at the last grid point, D is defined there as

$$(Df)_N = \frac{-f_{N-3} + 4f_{N-2} - 7f_{N-1} + 4f_N}{4}. \tag{101}$$

An extra half factor appears in this definition, compared with the one given in Ref. [51], because of the half factor in Υ_{NN}. Taylor expanding f_I for $I = N-3, \ldots, N$ at the Nth grid point and substituting all these expansions in the previous equation above gives us a series expansion of $(Df)_N$ with terms up to h^2 the same as given in Eq. (100), with $I = N$. As we will see shortly, our dissipation operator vanishes like h^3 as $h \to 0$. Also, the h^3 term in the Taylor expansion of $(Df)_I$ is zero for $I = 0, \ldots, N-1$ but nonzero for $I = N$. This residual term at the last grid point interferes with the dissipation operator and may cause the code to blow up from the outer boundary. Therefore, we redefine the operator D at the last grid point so that the h^3 term in $(Df)_N$ vanishes identically. This leads to the following definition of D at the last grid point:

$$(Df)_N = \frac{f_{N-4} - 5f_{N-3} + 10f_{N-2} - 11f_{N-1} + 5f_N}{4}. \tag{102}$$

Here also, an extra half factor is introduced because of the half factor in Υ_{NN}. Thus, the matrix form of D near the outer boundary is

$$D = \begin{pmatrix} \cdot & \cdot & \cdot & \cdot & \cdot & \cdot & \cdot \\ \cdot & 0 & 1/2 & 0 & 0 & 0 & 0 \\ \cdot & -1/2 & 0 & 1/2 & 0 & 0 & 0 \\ \cdot & 0 & -1/2 & 0 & 1/2 & 0 & 0 \\ \cdot & 0 & 0 & -1/2 & 0 & 1/2 & 0 \\ \cdot & 0 & 0 & 0 & -1/2 & 0 & 1/2 \\ \cdot & 0 & 1/4 & -5/4 & 5/2 & -11/4 & 5/4 \end{pmatrix}. \tag{103}$$

Now, using this definition of D and taking $\tilde{W}^- = \mathrm{diag}(\tilde{w}_0^-, \ldots, \tilde{w}_N^-)$ and $\tilde{B} = \mathrm{diag}(0, \ldots, 1/4)$, we define $\tilde{D}$ using Eq. (90). However, applying this operator to some smooth function f, one can see that the Taylor expansion of $(\tilde{D}f)_I$ not only violates the TEM property at $I = N-4, \ldots, N$, but also does not even give the leading term $h(\tilde{w}^- f)'/\tilde{w}^-$, which we will expect from the Sarbach method along with Eq. (87). Instead, looking at the

corresponding Taylor expansions, their leading terms are $\sim f/\tilde{w}^-$. Therefore, when divided by h, these terms will blow up at $\mathcal{I}^+$ with increasing resolution. To make the system consistent, we define the operator $\tilde{D}$ by hand. Using Eq. (83) in Eq. (87), we notice that D and $\tilde{D}$ are related as $\tilde{D} = (\tilde{W}^-)^{-1} D \tilde{W}^-$ in the bulk. Inspired from this, define $\tilde{D}$ on the whole grid as

$$\tilde{D} \equiv (\tilde{W}^-)^{-1} D \tilde{W}^-. \tag{104}$$

This gives

$$(\tilde{D}f)_I = \frac{(\tilde{w}^- f)_{I+1} - (\tilde{w}^- f)_{I-1}}{2\tilde{w}_I^-} = \frac{D(\tilde{W}^- f)_I}{\tilde{w}_I^-} \tag{105}$$

for $I = 0, \ldots, N-1$ and

$$(\tilde{D}f)_N = \frac{1}{4\tilde{w}_N^-}[(\tilde{w}^- f)_{N-4} - 5(\tilde{w}^- f)_{N-3} + 10(\tilde{w}^- f)_{N-2} - 11(\tilde{w}^- f)_{N-1} + 5(\tilde{w}^- f)_N] \tag{106}$$

for the term $I = N$. This definition of $\tilde{D}$ not only approximates Eq. (89) at second-order accuracy but also satisfies the TEM property at all grid points.

Since we are defining D and $\tilde{D}$ by hand and choosing $\tilde{W}^-$ by Sarbach's method, in order to incorporate the SBP property, we calculate the boundary matrix $\tilde{B}$ using Eq. (96). We do not need to worry about the relation (97), as it is automatically satisfied by this new choice of D and $\tilde{D}$. Unlike what was assumed so far, this new $\tilde{B}$ has nonzero entries in the bulk as well as at the outer boundary; i.e., we also have $\tilde{B}_{IJ} \neq 0$ for both $I, J < N$. However, we realize from Eq. (94) that only the symmetric part of $\tilde{B}$ contributes to the energy flux. Interestingly, it turns out that the symmetric part of the new $\tilde{B}$ has nonzero entries only at (I, N) and (N, I) positions, with $I = (N-4), \ldots, N$.

In summary, we initially chose the operator D, the weight matrix $\tilde{W}^-$, and the boundary matrix $\tilde{B}$ by hand and derived $\tilde{D}$ using the SBP relation (90). Doing this, we lost all control over the properties of $\tilde{D}$ near the outer boundary. As a result, we obtained a form of $\tilde{D}$ which is inconsistent with Eq. (89) near the outer boundary. In order to resolve this issue, we adopted the reverse strategy. We first chose D and $\tilde{D}$ satisfying the TEM property everywhere and $\tilde{W}^-$ from Sarbach's method, which we preferred over the Evans' method. Using these operators, we then used the SBP property to calculate the boundary matrix $\tilde{B}$. Since $\tilde{B}$ merely gives the energy flux at the outer boundary, the price we pay in order to incorporate both SBP and TEM properties is that we lose control over the boundary flux.

Another method for incorporating TEM could be adapted from Ref. [50], which employs the outer boundary condition in the SBP scheme in $1+1$ dimensions. Demanding specific relations between the weight and boundary matrices between $1+1$ and $(j+1)$ dimensions, they derive the operator $\bar{D}$ in $j+1$ dimensions. In our setup, we instead saw how D and $\tilde{D}$ are related without invoking a $1+1$-dimensional system. Given the above, we expect that our method generalizes for any spatial dimension.

F. The SBP-TEM and SBP-Stable methods

In this section, we give two numerical schemes, obtained by approximating the continuum equations at the outer boundary in two different ways. We will compare both in our numerical experiments and see that they, empirically, give satisfactory norm convergence but have slightly different pointwise convergence. It is observed empirically in many cases that the first scheme, which we call the SBP-TEM discretization, gives perfect pointwise convergence but is not formally stable. The second scheme, the SBP-Stable scheme, is provably stable but has a lower-order pointwise errors near the outer boundary.

1. SBP-TEM

As before, the total change in energy is given by

$$\dot{\tilde{E}} = -\frac{1}{2}\tilde{w}_N^- F_N \frac{2R'_N}{2R'_N - 1}\tilde{\Psi}_N^2 + (\tilde{\Sigma}^+)^T P \tilde{B} P \tilde{\Sigma}^+ - \frac{1}{2}\tilde{w}_N^- P_N^2 (\tilde{\Sigma}_N^+)^2 - (\tilde{\Sigma}^-)^T \tilde{B} \tilde{\Sigma}^- - \frac{1}{2}\frac{1}{2R'_N - 1}\tilde{w}_N^- (\tilde{\Sigma}_N^-)^2, \tag{107}$$

where the first, third, and fifth terms arise because of the moving outer boundary. The boundary matrix $\tilde{B}$ here is the one obtained by using the SBP and TEM properties.

Defining $\tilde{B}_s := (\tilde{B} + \tilde{B}^T)/2$, we observe that only the last row and the last column of $\tilde{B}_s$ are nonzero. As $r_o \to r_{\mathcal{I}}$, $P_N = 1/\chi_N \to 0$ and $1/(2R'_N - 1) \to 0$. Thus, the second, third, and fifth terms in Eq. (107) vanish, as all other factors in these terms are $O(1)$. The second term vanishes, because $\tilde{B}_s$ has nonzero elements only in its last row and last column. Since P is diagonal, multiplying P on the left of $\tilde{B}_s$ gives the matrix $P\tilde{B}_s$ with all elements zero in its last row and nonzero elements only in its last column. Multiplying $P\tilde{B}_s$ on the right by P gives all elements zero in the last column of the resulting matrix. This gives $P\tilde{B}_s P = 0$. Therefore, the total change in energy reduces to

$$\dot{\tilde{E}} = -\frac{1}{2}\tilde{w}_N^- F_N \frac{2R'_N}{2R'_N - 1}\tilde{\Psi}_N^2 - (\tilde{\Sigma}^-)^T \tilde{B}_s \tilde{\Sigma}^-, \tag{108}$$

which is analogous to (108) in the continuum problem. Here there is, however, an important subtlety. The first term does indeed directly map to the potential term on the

right-hand side of Eq. (108). But the second contains cross terms between points at the boundary and points in the interior. In this sense, one might argue that the SBP-TEM scheme is not truly an SBP discretization, but we nevertheless keep the name to indicate the origin of the method. This shortcoming means that there is a deviation of the discrete energy flux at $\mathscr{I}^+$ from the continuum one. To understand this deviation, we ignore the potential term. Expanding $\tilde{B}_s$ then, we get

$$\begin{aligned}\dot{\tilde{E}}(t) = &-\frac{5}{4}\tilde{w}_N^-(\tilde{\Sigma}_N^-)^2 + \Big[\frac{9}{8}(\tilde{w}_{N-1}^- + \tilde{w}_N^-)\tilde{\Sigma}_{N-1}^- \\ &-\frac{5}{4}(\tilde{w}_{N-2}^- + \tilde{w}_N^-)\tilde{\Sigma}_{N-2}^- + \frac{5}{8}(\tilde{w}_{N-3}^- + \tilde{w}_N^-)\tilde{\Sigma}_{N-3}^- \\ &-\frac{1}{8}(\tilde{w}_{N-4}^- + \tilde{w}_N^-)\tilde{\Sigma}_{N-4}^-\Big]\tilde{\Sigma}_N^-. \end{aligned} \tag{109}$$

We can furthermore rewrite this expression by separating the continuum part out from this expression to obtain

$$\dot{\tilde{E}}(t) = -\frac{1}{2}\tilde{w}_N^-(\tilde{\Sigma}_N^-)^2 - \tilde{\Sigma}^-\tilde{W}^-(\Delta^2 + \tilde{\Delta}^2)\tilde{\Sigma}^-, \tag{110}$$

where $\Delta^2\tilde{\Sigma}_I^- = 0$ for $I = 0, \ldots, N-1$,

$$\Delta^2\tilde{\Sigma}_N^- = \frac{\tilde{\Sigma}_{N-4}^- - 5\tilde{\Sigma}_{N-3}^- + 10\tilde{\Sigma}_{N-2}^- - 9\tilde{\Sigma}_{N-1}^- + 3\tilde{\Sigma}_N^-}{8}, \tag{111}$$

and finally

$$\tilde{\Delta}^2 = (\tilde{W}^-)^{-1}\tilde{\Delta}^2\tilde{W}^-. \tag{112}$$

At the last grid point, the operator Δ^2 corresponds to the continuum operator

$$\Delta^2 f = \frac{h^2}{8}\left(f'' + \frac{h^4}{12}f^{(4)} + \cdots\right). \tag{113}$$

Assuming convergence, this gives

$$\dot{\tilde{E}}(t) = -\frac{1}{2}\tilde{w}_N^-(\tilde{\Sigma}_N^-)^2 - h^2(\cdots), \tag{114}$$

as resolution increases, so that the deviation diminishes like h^2, consistent with the TEM property.

Therefore, convergence of the SBP-TEM scheme is the only remaining aspect to prove. A standard way to do so is to first prove stability and then use the Lax equivalence theorem [49,52] to ensure convergence. Unfortunately, the quadratic form in $\tilde{\Sigma}^-$ on the right-hand side of Eq. (109) is not sign definite, and so formal stability does not follow. This implies that the energy at any later hyperboloidal time slice is not (in general) upper bounded by that on the initial slice. It is important to realize that this shortcoming does not mean that the method will not converge for any given initial data. Rather, it means that there is no *guarantee* of convergence. It would be interesting to know the specific class of data that does converge. To find examples of "bad" data, we need to look at the eigenvectors of the boundary matrix associated with positive eigenvalues. Instead of going into more detail along these lines, in Sec. V, we study empirically convergence of the scheme for various choices of initial data.

2. SBP-Stable

We now present an alternative discretization which gives a provably stable numerical scheme but requires a drop in the pointwise convergence order at the outer boundary. This scheme is obtained by adding $A\tilde{\Sigma}^-$ to the right-hand side of $\dot{\tilde{\Sigma}}^-$ in Eq. (92), with

$$A = \Upsilon(\Upsilon^{-2}\Delta^2 + \Upsilon^{-2}\tilde{\Delta}^2). \tag{115}$$

This adds a new term in Eq. (108), which is

$$(\Sigma^-)^T\Upsilon\tilde{W}^-A\tilde{\Sigma}^-. \tag{116}$$

Since only the symmetric part of $\Upsilon\tilde{W}^-A$ contributes to $\dot{\tilde{E}}$, when added to $\tilde{B}_s$, it gives

$$-\tilde{B}_s + \frac{\Upsilon\tilde{W}^-A + (\Upsilon\tilde{W}^-A)^T}{2} = \mathrm{diag}(0, \ldots, -\tilde{w}_N^-/2), \tag{117}$$

and so, for this adjusted scheme, we get $\dot{\tilde{E}} = \dot{E}$, the continuum energy decay rate, which is negative semidefinite, and the resulting semidiscrete scheme is stable. Choosing a suitable time integrator, we can make the whole discrete scheme stable. Therefore, by the Lax equivalence theorem, the resulting scheme is convergent. However, Eq. (115) shows that the $A\tilde{\Sigma}^-$ term vanishes like h rather than h^2 with increasing resolution. Thus, it decreases the convergence order of the numerical scheme. We call $A\tilde{\Sigma}^-$ an "artificial boundary" term, as it vanishes in the continuum limit.

When the outer boundary is not at $\mathscr{I}^+$, we need to add more such artificial boundary terms to the equations. Interestingly, it turns out that adding these terms to the discrete equations of motion is equivalent to rather changing the definition of D at the outer boundary:

$$(Df)_N = \frac{f_N - f_{N-1}}{2}. \tag{118}$$

The operator $\tilde{D}$ is automatically redefined from Eq. (104), when D is defined by Eq. (81) for $I = 0, \ldots, N-1$ and Eq. (118). This clarifies how these artificial boundary terms are decreasing the accuracy of the numerical scheme at the outer boundary, effectively by decreasing the accuracy of D and $\tilde{D}$ at the last grid point. Therefore, just to keep the

generality, we will drop the accuracy of D and $\tilde{D}$ instead of using the artificial boundary terms. This result is unique, because the choice of artificial boundary terms depends uniquely on the definition of D and $\tilde{D}$ at the last grid point and demanding that Eq. (117) is satisfied.

Interestingly, dropping the accuracy of D and $\tilde{D}$ does not affect the norm convergence. As we saw above, this is equivalent to using D and $\tilde{D}$ satisfying the TEM property and adding suitable artificial boundary terms. Since these artificial boundary terms in the equations vanish like h with increasing resolution, we can infer from Eqs. (115) and (116) that their contribution to $\dot{\tilde{E}}$ vanishes like h^2. Therefore, the norm of errors should still converge at second-order accuracy. On the other hand, the artificial boundary terms do run the risk of badly damaging pointwise convergence, as they may reflect a lot of noise into the bulk.

The remaining ingredients required for the implementation of our discretized scheme are the treatment of the origin, the adjustment of the energy, and the addition of dissipation. As they are slightly more technical, they are presented in Appendixes A, B, and C, respectively.

V. NUMERICAL EVOLUTION

A. Code description

We employ a one-dimensional code, written for spherically symmetric systems in spherical polar coordinates on hyperboloidal slices, using the same infrastructure as that of the work in Refs. [15,16,53]. We use a compactified radial coordinate and hyperboloidal time as explained in Sec. II. The implementation uses the method of lines with a fourth-order Runge-Kutta for time integration. We work with second-order accurate finite-difference operators D and $\tilde{D}$ to approximate the spatial derivatives derived from the SBP-TEM scheme, as given by (81), (102), (105), and (106), and the SBP-Stable scheme, as explained in Sec. IV F 2. Our spatial grid has grid points at the origin and at $\mathscr{I}^+$, as shown in Fig. 3. Regarding dissipation (see Appendix C for the full details), we use a fourth-order Kreiss-Oliger-like dissipation operator Q_{d2} satisfying the TEM property, given by (C1), (C14), and (C15), with the SBP-TEM scheme and by the operator $\mathbf{Q}$ acting on the whole state vector and satisfying the dissipative property (DP), as constructed in Sec. C 2, with the SBP-Stable scheme. We treat the origin as an inner grid point, for which we introduce ghost points on its left with the same grid spacing as on the physical grid, and populate them using the parity conditions (A2). Then all the finite-difference operators at the origin are defined in the same way as on a typical interior grid point, using a centered stencil; cf. Fig. 3. It suffices to have a single ghost point in order to define D and $\tilde{D}$ at the origin, but we need two such ghost points to define the dissipation operators there. In contrast, the outer boundary is a true boundary which is placed at $\mathscr{I}^+$. All the operators defined there are completely left sided.

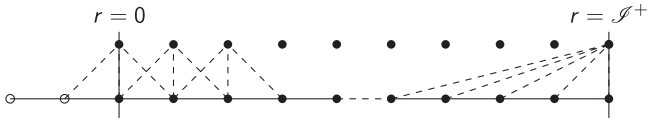

FIG. 3. A schematic diagram showing the nonstaggered grid and second -order finite-difference stencils (dashed line segments) that we use in the numerical implementation. All the grid points are uniformly spaced. The stencil is centered everywhere except on the boundary, which is at $\mathscr{I}^+$, where it leans left and uses five grid points in the SBP-TEM scheme and two for the SBP-Stable one. The values of the variables on the black-filled points are evolved using the equations of motion. The empty circles on the left denote the ghost points, which are required to calculate derivatives at the origin and are filled using the parity conditions described in Appendix A.

B. Implementation

We experimented with various different values of the compactification parameter n, defined in Eq. (3), obtaining qualitatively similar results. For brevity, in our presentation we choose the compactification function $\Omega(r)$ given by Eq. (A4) with $n = 2$ and $r_{\mathscr{I}} = 1$. We observe that using Evans' method at the origin gives both the pointwise and norm convergence plots visually indistinguishable from those obtained by rewriting the equations there using the l'Hôpital rule. This is exactly what we expect from the explanations given in Appendix A. In our implementation, we use the l'Hôpital rule, as it has an advantage that the energy norm becomes independent of the resolution. We set the height function H such that $H'(R(r)) = 1 - 1/R'(r)$. We use $\chi = \sqrt{1+R^2}$ as a rescaling function and $\gamma_2 = 0$ for all our purposes, as justified in Sec. IV D 3. We take $N = 200$ as our base resolution and increase this number by a factor of 2 whenever performing convergence tests. This gives $h = r_{\mathscr{I}}/N = 0.005$ at the original resolution. The Courant-Friedrichs-Lewy factor, defined as the ratio between the time step and grid spacing $\delta t/h$, is taken to be 0.5 unless stated otherwise. We work with the $(\tilde{\Psi}, \tilde{\Sigma}^+, \tilde{\Sigma}^-)$ system for all three choices of F considered here. We have tested several families of initial data, but, in our presentation, we take

$$\psi(0,R) = ae^{-\lambda R^2} \quad \text{and} \quad \pi(0,R) = 0, \tag{119}$$

with $a = 0.01$ and $\lambda = 1$, unless stated otherwise, and compute the initial data for the $(\tilde{\psi}, \tilde{\sigma}^+, \tilde{\sigma}^-)$ variables according to the transformation rules (10) and (17).

C. Results and interpretation

1. Linear wave equation, $F = 0$

Without adding dissipation, the evolved variables look quite noisy at the origin, for both SBP-TEM and

SBP-Stable schemes. The reason for the noise is most likely the nonsmoothness, mentioned in Appendix A, that arises from our choice of χ in combination with our parity conditions. Since our primary interest is in the regularization at $\mathscr{I}^+$, and in the future we will employ a multipatch method that avoids the coordinate singularity at the origin, we have not invested a huge effort in improving the treatment there. Instead, we use a small amount of dissipation to suppress the noise. Interestingly, setting for the dissipation parameter $\epsilon = 0.002$ suffices to damp almost all of this noise by $t = 2$; with this level of dissipation, the amplitude of the solution at our base resolution is down to $\sim 10^{-8}$ by $t = 10$.

Each of our schemes is naturally associated with a different dissipation operator, SBP-Stable with the dissipation operator $\mathbf{Q}$, which acts on the whole state vector and satisfies the DP, and SBP-TEM with Q_{d2}, which acts variable by variable and has clean pointwise properties. If we use instead $\mathbf{Q}$ with SBP-TEM, we see that pointwise convergence is damaged, whereas if we use Q_{d2} with SBP-Stable, we see at particular times a small, though convergent, growth in the energy of the solution. Matching the dissipation operators with their natural discretization plays to the strengths of each of the two methods and works well.

Returning to Fig. 1, we see the basic behavior of the massless scalar field satisfying the LWE in our simulations. The initial narrow pulse at the origin, chosen to be Gaussian-like as in Eq. (119) with $a = 0.01$ and $\lambda = 100$, propagates to $\mathscr{I}^+$ with speed equal to unity, as expected from our construction in Sec. II. Here, we plot the absolute value of the rescaled field $|\tilde{\psi}|$. The plot shows two bursts of the pulse because of the time symmetry in our initial data obtained by taking $\pi(T = 0, R) = 0$. Most of the region looks white, because for clarity we show only the values for $10^{-6} < |\tilde{\psi}| < 10^{-3}$. This plot was generated using the SBP-Stable scheme with a little ($\epsilon = 0.002$) dissipation. This plot also shows a small amount of noise at the origin which gets damped with time because of the dissipation.

In order to test the correctness of the implementation, we compare the decay rate over time of our approximation to the physical energy (93) with that of the analytical one. Complete agreement between the two is demonstrated in Fig. 4 for the SBP-Stable scheme. To generate these curves, we consider the general solution of the LWE in spherical symmetry:

$$\psi(T, R) = \frac{f(T + R) - f(T - R)}{R} \tag{120}$$

and then rewrite it in terms of hyperboloidal coordinates and choose $f(x) = e^{-x^2}$. With this f, we build the initial data for the corresponding numerical setup. The numerical solution plotted is constructed at our lowest resolution, $N = 200$.

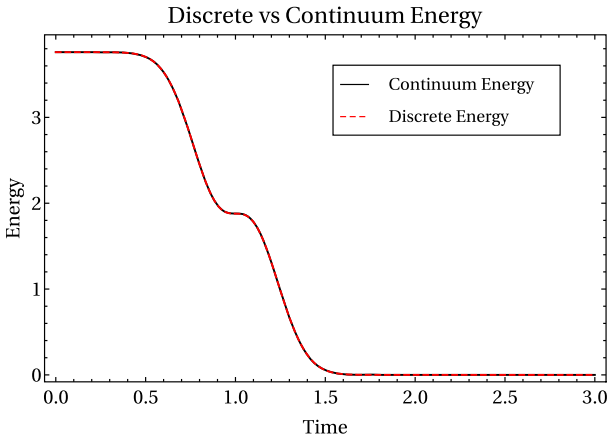

FIG. 4. Comparison of the continuum and discrete energies as a function of time for the initial data specified in the main text. These are the same data as plotted in Fig. 1, and so it makes sense that, as each of the two pulses hits the outer boundary, the energy drops rapidly.

We now compare the SBP-TEM and SBP-Stable schemes through the norm and pointwise convergence curves with a specific focus on $\mathscr{I}^+$. The norm convergence plots in the adjusted norm (B1), described in detail in Appendix B, are shown in Fig. 5 for the two schemes, plotted in different colors, and for different resolutions plotted in solid and dashed curves. At late times, a small, smooth, stationary, though convergent feature remains in Ψ (not shown here). We interpret this as the constraint violation induced by the dissipation. This violation

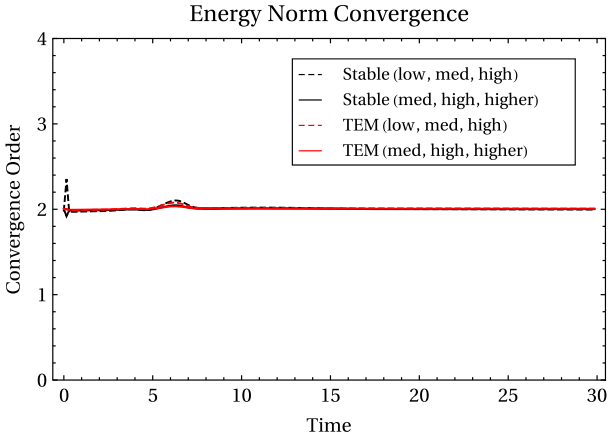

FIG. 5. Convergence order of our scalar field obeying LWE in the adjusted energy norm given by Eq. (B1). The red curves show the same for the SBP-TEM discretization and the black curves for the SBP-Stable one. Both are near perfect, although it is true that the SBP-Stable plot would not be as clean if we focused on the physical energy (93) instead, because, as can be understood from Fig. 4, the energy present after $t \sim 3$ is negligible, and the effects of dissipation start to dominate the error in $\tilde{\Sigma}^{\pm}$ after around $t \sim 7$.

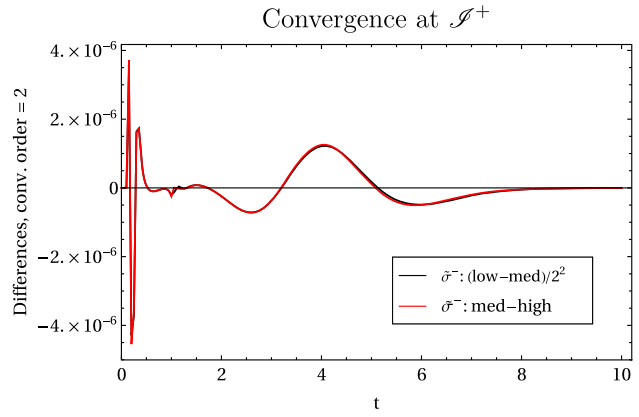

FIG. 6. Convergence of $\tilde{\sigma}^-$ at $\mathcal{I}^+$ for the scalar field obeying the LWE in the SBP-Stable discretization.

dominates the other errors by about 3 orders of magnitude toward the end of the evolution. Figure 5 shows almost perfect second-order convergence for all times in both schemes, as expected.

If we construct a similar plot using the physical energy (93), that is, without adding the $\tilde{\Psi}^2$ term, the stationary error is completely eliminated and the remaining errors start dominating. In the SBP-TEM scheme, all these remaining errors still converge at second order, and we again observe a perfect second-order norm convergence with only small wiggles in some time intervals. These wiggles are observed to be completely dependent on the dissipation, as increasing the dissipation parameter ϵ increases their amplitude. Since these errors converge faster than those produced by the SBP-TEM scheme, these wiggles diminish rapidly by increasing the resolution. On the other hand, in the SBP-Stable scheme, this convergence order starts drifting to ∼3 at late times. This is because, at late times, errors introduced by the dissipation operator start dominating. Although these errors converge like h pointwise at the last three grid points (cf. Sec C 1), they can be easily seen to converge like h^3 in the norm. This appears to be the price for guaranteed stability. We do not observe this behavior in the SBP-TEM scheme, because in this scheme the energy flux through $\mathscr{I}^+$ depends on the resolution.

We now consider pointwise convergence. Since the SBP-TEM scheme is designed to converge at second order at all grid points for suitable initial data, we expect all the errors to converge pointwise like h^2 even at $\mathscr{I}^+$, at least for a large class of initial data. On the other hand, the SBP-Stable scheme uses various finite-difference operators at the last grid point, some of which are only $O(h)$, so we might expect a decline in convergence order in this scheme at $\mathscr{I}^+$. Interestingly, this is not what we observe. Figure 6 shows clean second-order convergence of $\tilde{\sigma}^-$ at $\mathscr{I}^+$ in the SBP-Stable scheme, and we obtain similar results for $\tilde{\psi}$ and $\tilde{\sigma}^+$. The equivalent plot for the SBP-TEM scheme looks even better. We observe with that scheme a smaller amplitude of the error at $\mathscr{I}^+$ by about a factor of 2.

In Fig. 7, we compare pointwise convergence in the two different schemes. The top row shows the pointwise convergence curves in the SBP-TEM scheme at three different instants, the bottom the equivalent plots with the SBP-Stable scheme. The first column shows how the noise at the origin dominates the errors generated on the rest of the grid. We expect that this source of error could be reduced by adjusting χ to obtain smoothness at the origin. At this instant, both sets of curves look essentially the same. In the second column, we show equivalent plots at some intermediate time when we observe a small wiggle on the

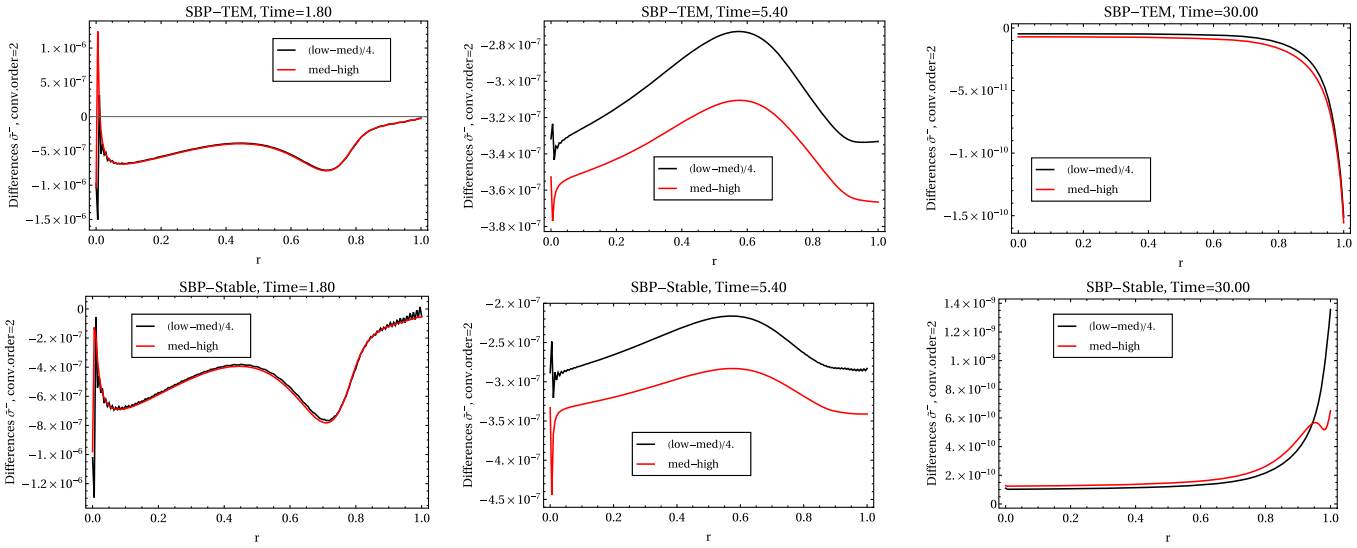

FIG. 7. Pointwise convergence of the scalar field obeying the LWE. The upper row shows the plots obtained from the SBP-TEM discretization scheme at $t = 1.8$, 5.4, and 30, and the bottom lower row shows the equivalent plots obtained from the SBP-Stable scheme. We can observe how at late times the outer boundary starts affecting the pointwise convergence in the SBP-Stable scheme.

norm convergence plot. As described before, this wiggle is there due to the errors introduced by the dissipation operator. At this instant, which corresponds to the small wiggle in the convergence plot in Fig. 5, we can see that the plots for both schemes do not overlap. In the last column, we see a typical pointwise convergence behavior at late times. The bottom right plot explains the deviation in the norm convergence in the SBP-Stable scheme in the physical energy. These last panels clearly demonstrate the superiority of the SBP-TEM scheme over the SBP-Stable one at late times on this initial data.

While working with the continuum equations, if we start with constraint-satisfying initial data, the equations of motion assure that the constraint (98) in the analytic solution is satisfied for all times. However, in the discrete case, the constraint (99) is violated even for the initial data. This violation is approximated in our scheme as

$$\hat{\mathcal{C}}_I = \frac{1}{2R'_I - 1}\left(\frac{h^2}{6}\Psi'''_I + \cdots\right), \tag{121}$$

for $I = 0, \ldots, N$. Therefore, we expect the constraint violation to converge at second order. In Sec. IV D 3, we showed that, in the absence of dissipation, $\dot{\hat{\mathcal{C}}} = 0$, independent of the choice of the discretization scheme. Adding dissipation terms to our equations, however, leads to a nontrivial form of $\dot{\hat{\mathcal{C}}}$. This is exactly what we observe in our numerical results. For $\epsilon > 0$, a near-stationary constraint violation appears on the grid, slowly evolving because of the dissipation but vanishing with increasing resolution.

2. Linear wave equation with potential, $F = 1/\chi^2$

The system $F = 1/\chi^2$ and other models with potentials are interesting for our methods for the following reason. In spherical symmetry, Eq. (6) expressed in terms of the null coordinates $u = T - R$ and $v = T + R$ shows that the rescaled field $\bar{\psi} = R\psi$ satisfies the equation

$$\partial_u\partial_v\bar{\psi} = \partial_v\partial_u\bar{\psi} = -F\bar{\psi}. \tag{122}$$

Since, in spherical symmetry, $\partial_u\bar{\psi}$ and $\partial_v\bar{\psi}$ represent the characteristic variables, respectively, the above equation simply means that all the "outgoing modes" of $\bar{\psi}$, and, hence, of ψ, are coupled to all the incoming ones via the potential, and vice versa. This coupling is dangerous in the hyperboloidal setup, because if high-frequency incoming modes are generated near $\mathscr{I}^+$, they will necessarily be poorly resolved on the grid. We are now considering $F = 1/\chi^2$, where the coupling, which is completely absent in the LWE, decreases with increasing radius like $1/R^2$ and is, hence, absent at the last grid point. In the next section, we consider a much more extreme example.

Figure 8 shows the convergence order in the energy norm of the field obeying the LWEP with $F = 1/\chi^2$. In this case,

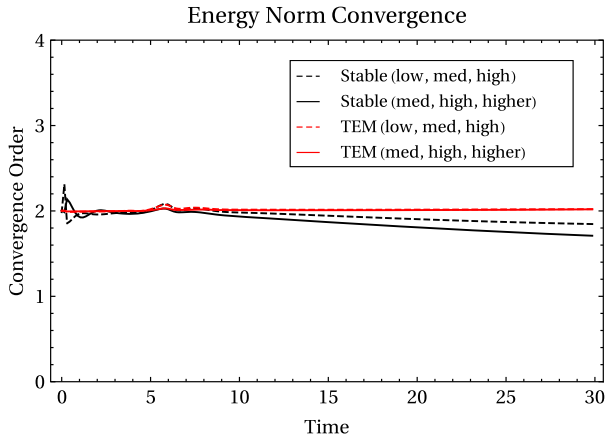

FIG. 8. Convergence order of the scalar field obeying the LWEP with $F = 1/\chi^2$ in the energy norm given by Eq. (93). In this particular case, we simply use the physical energy, because it is not degenerate near infinity. The red curves correspond to the SBP-TEM discretization and the black curves to the SBP-Stable one.

we observe an almost perfect convergence order at all times in the SBP-TEM scheme. However, the convergence order slowly decays in the SBP-Stable scheme once the data are very small and the error is dominated by the lower-order operators (in the derivatives and dissipation) near the outer boundary. This plot also demonstrates the superiority of the SBP-TEM scheme over the SBP-Stable one for this family of initial data. However, we also observe very good second-order convergence at $\mathscr{I}^+$ in both schemes, appearing very similar to that shown in Fig. 6.

Here, in contrast to the plain wave equation even given initial data of compact support, part of the physical signal always remains on the computational domain. The reason for the slower decay of the solution is the coupling between the incoming and outgoing modes of the solution as described above. Therefore, as in Price's law [54], we expect a late-time tail at $\mathscr{I}^+$ which decays like an inverse power of time t. This is what we observe in Fig. 9, which is constructed from the SBP-TEM scheme. We can see a perfect overlap of the curves corresponding to three different resolutions for long times, up until $t = 50$ in the plot. As could be anticipated from the previous figure, however, this overlap is not as good in the SBP-Stable scheme. This result again demonstrates the superiority of the SBP-TEM scheme over the SBP-Stable setup for these initial data.

3. Linear massive Klein-Gordon equation, $F = m^2$

As an extreme example, we now consider the alternative potential $F = m^2$ with no decay near infinity. Despite the fact that the hyperboloidal form of the equations of motion (22) have terms with divergent coefficients of the form $R'F\tilde{\psi}$ near infinity, the continuum equations still make sense, at least within a large class of initial data, because solutions decay faster than any inverse polynomial in R

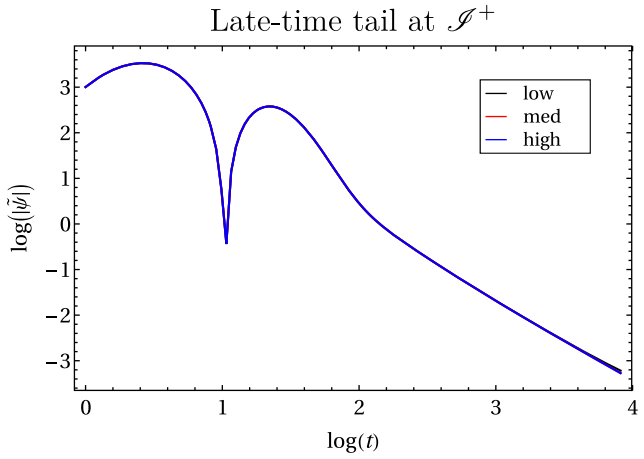

FIG. 9. Late-time tail of a scalar field obeying the LWEP with $F = 1/\chi^2$ at three different resolutions, with $N = 200$, 400, and 800, respectively. This plot is generated for the initial data given by Eq. (119) with $a = 100$ and $\lambda = 1$. The slope of this tail is measured to be ≈ -1.74.

[25,55]. A separate question is whether or not we are able to find accurate approximate solutions in our coordinates. Even given a usable setup with a conserved positive energy at the semidiscrete level, such an energy would require a restricted class of initial data that decay rapidly at infinity, and so formal numerical stability [49] does not automatically follow. Perhaps an alternative perspective is that the mass term is effectively arbitrarily "stiff" near infinity, so that problems in time integration could be foreseen.

We choose initial data for $\tilde{\psi}$ that fall off fast enough so that $R'\tilde{\psi} \to 0$ as $r \to r_{\mathscr{I}}$, which, according to the continuum estimates mentioned above and as can be deduced from Eq. (30), should then hold true at later times. The initial data given by Eq. (119) are one such choice. Under this assumption, all variables must vanish at $\mathscr{I}^+$. Unfortunately, because of the singular coefficient, neither of our two schemes can be used without modification. We have thus tried various different strategies to manage the singular coefficients, including, for example, fixing all time derivatives at $\mathscr{I}^+$ to vanish. By so doing, we are able to perform numerical evolutions and obtain very good energy conservation, even at low resolutions. But, unfortunately, as soon as an outgoing pulse hits the region near $\mathscr{I}^+$, both norm and pointwise convergence are completely lost, as high-frequency reflections propagate back into the central region. Performing convergence tests at successively higher resolutions does not help.

Presently, it is not clear how, or even if, these difficulties can be overcome. One possibility to obtain at least a consistent scheme with a semidiscrete energy estimate would be to impose Dirichlet-type boundary conditions at a finite timelike boundary and to then take the limit to $\mathscr{I}^+$. But, as mentioned above, even that would not guarantee convergence. Another strategy might be to build a discretization around the Bessel functions which naturally capture the structure of solutions [25]. Final possibilities would be to maintain a central, flat, slicing over the region of interest for the massive field or to simply admit defeat and modify the field equations near $\mathscr{I}^+$.

VI. CONCLUSIONS

In this series [17,19,20] of papers, we are developing a method to attach future null infinity to the computational domain via hyperboloidal slices in numerical relativity. There are several aspects to the problem. In the present work, we have focused on the properties of two approximation schemes for first-order reductions of linear wave equations. We call these approximations SBP-Stable and SBP-TEM. The first of these is formally stable, while the second is instead built so that troublesome reflections from null infinity are minimized. Here we worked in spherical symmetry with second-order accurate operators, but neither of these simplifications was fundamental. We moreover expect that both schemes can be straightforwardly lifted to treat nonlinear equations.

In our numerical experiments, the two schemes behave comparably in many tests. Although the SBP-TEM method is not formally stable even for the flat-space wave equation, it seems unlikely that the user would stumble across the expected class of "bad" initial data in practice. If they did, the SBP-Stable method could be applied instead. Concerning the SBP-Stable method, we seem to be forced to use low-order operators near the outer boundary. In long evolutions, the errors associated with these operators are dominant. On the other hand, we were positively surprised when using the SBP-Stable method that pointwise convergence there is not too badly damaged for most of the evolution.

The hyperboloidal coordinates that we employ are fundamentally adapted to the clean resolution of outgoing waves. There is, therefore, a limited class of models that can be accurately treated by their use. We might anticipate, for example, that any model which generated large amounts of incoming radiation near null infinity to be poorly approximated by either of our schemes. To investigate this, we studied wave equations with different potentials. We found that, when the potential decays sufficiently fast near null infinity, our methods serve their purpose well, but when this is not the case, as in the massive Klein-Gordon equations, they cannot be directly applied and, at least with naive adjustment, fail badly. Interestingly, even if a consistent method with a conserved norm could be found at the semidiscrete level, it would not necessarily converge, because the equations of motion do not regularize. In the future, it will be desirable to unpick the relationship between the generation of incoming radiation and the possibility to regularize a given model. It would also be interesting to understand the slowest possible decay of a potential that could be well treated by our (or any other) methods.

An important open question is whether or not *any* scheme could be given that combines the advantages of both the SBP-Stable and SBP-TEM setups, perhaps building on Refs. [56,57] and using a careful upwinding discretization. Taking a broader view, it would be highly desirable to understand if, or how, the energy method used here could be combined with alternative novel discretization schemes, such as those proposed in Refs. [58–61], to demonstrate stability on hyperboloidal slices. For now, however, our highest priority is to combine the methods we have developed here with the regularization given in Ref. [20] for nonlinear models to treat GR proper.

ACKNOWLEDGMENTS

We are grateful to Abhay Ashtekar, Sanjeev Dhurandhar, Edgar Gasperin, Jayant V. Narlikar, and especially Miguel Zilhão for useful discussions. This work was supported through the European Research Council Consolidator Grant No. 647839, the FCT Programs IF/00577/2015, PTDC/MAT-APL/30043/2017, the Ph.D. researcher Decree-Law No. 57/2016 (Portugal), and Project No. UIDB/00099/2020. All authors thank Navajbai Ratan Tata Trust (NRTT) grant for supporting various visits of the authors to IUCAA and S. G.'s visit to CENTRA, Técnico, Lisboa.

APPENDIX A: ORIGIN

In order to calculate various derivatives at the origin, which we treat as an interior point, using centered finite difference stencils, we introduce ghost points to the left of the origin in our numerical grid; see Fig. 3. We fill these ghost zones using the suitable parity conditions

$$\tilde{\psi}_{-I} = \tilde{\psi}_I, \quad \tilde{\pi}_{-I} = \tilde{\pi}_I, \quad \text{and} \quad (\tilde{\phi}_R)_{-I} = -(\tilde{\phi}_R)_I \tag{A1}$$

or, equivalently,

$$\tilde{\psi}_{-I} = \tilde{\psi}_I, \qquad \tilde{\sigma}^+_{-I} = \tilde{\sigma}^-_I, \quad \text{and} \quad \tilde{\sigma}^-_{-I} = \tilde{\sigma}^+_I, \tag{A2}$$

where $\chi_I = \sqrt{1+R_I^2}$. These parity conditions are obtained by using the rescaling (17) for $r \geq 0$ and $\tilde{\psi} \equiv \chi\psi$, $\tilde{\sigma}^+ \equiv \chi\sigma^+$, and $\tilde{\sigma}^- \equiv \chi^2\sigma^-$ for $r < 0$. The latter rescaling gives all the rescaled variables $O(1)$ for all $r < 0$ as σ^+ becomes the outgoing characteristic variable for $r < 0$, and hence falls like $1/R$, and σ^- becomes the incoming one, and hence falls like $1/R^2$. Note that this extension renders the evolved fields nonsmooth at the origin, a shortcoming that could be easily overcome by adjusting the rescaling slightly. This could be done, for example, by choosing χ to be 1 identically in a neighborhood of the origin. Since we are concerned primarily with the behavior of the approximation near infinity, we do not do so and will instead rely on artificial dissipation to suppress any noise produced. The above parity conditions are appropriate if and only if R is taken to be an odd function of r and H an even function of R. For $r \geq 0$, $H'(R(r)) = 1 - 1/R'(r)$ gives $H(r) \equiv H(R(r)) = R(r) - r$. To impose evenness, we must define H by

$$H(r) = \begin{cases} R(r) - r, & \text{for } r \geq 0, \\ r - R(r), & \text{for } r < 0. \end{cases} \tag{A3}$$

Moreover, for $r < 0$, we must take $c_- = -1$ and $c_+ = 1/(2R' - 1)$, as c_+ and c_- switch roles as incoming and outgoing coordinate light speeds, respectively. Taking R defined by Eq. (3), we see that $H(r)$ is only C^1 at the origin. This is problematic, because due to this we can never expect a smooth evolution of the fields at the origin. To overcome this problem, we redefine $\Omega(r)$ as given in Eq. (3) by

$$\Omega(r) = 1 - \frac{1}{2}\frac{r^2}{r_{\mathcal{F}}^2}\left[\tanh\left\{\tan\left(\pi\left(\frac{r}{r_{\mathcal{F}}} - \frac{1}{2}\right)\right)\right\} + 1\right]. \tag{A4}$$

This choice of $\Omega(r)$ not only has similar asymptotics to the compactification function as the one defined in Eq. (3) but also gives $R^{(m)}(0) = 0$ for every integer $m > 1$, as $\Omega^{(m)}(0) = 0$ for $m \geq 1$. Therefore, the height function $H(r)$ so obtained is C^∞ at the origin with $H^{(m)}(0) = 0$ for all $m \geq 0$.

Since there is a $1/R$ singularity at the origin, there are two methods to tackle it. One is using l'Hôpital's rule and the other is using Evans' method, as described before. Using l'Hôpital's rule, we completely get rid of the operator $\tilde{D}$ at the origin, whereas, using Evans' method, we get the value of $\tilde{w}_0^-$ given by

$$\tilde{w}_0^- = \frac{(DR^3)_0}{6hR_0'(1+R_0^2)} = \frac{R_1^3 - R_{-1}^3}{12hR_0'(1+R_0^2)} = \frac{R_1^3}{6h}. \tag{A5}$$

This form of $\tilde{w}_0^-$ has the following series expansion:

$$\tilde{w}_0^- = \frac{1}{6R_0'(1+R_0^2)}\left[(R_0^3)' + \frac{h^2}{6}(R_0^3)''' + \cdots\right] = \frac{h^2}{6}. \tag{A6}$$

The series terminates, because $R_0 = 0$, $R_0' = 1$, and $R^{(m)}(0) = 0$ for every integer $m > 1$. Therefore, defining $\tilde{w}_I^-$ using Sarbach's for every $I \neq 0$ and Evans' method to define $\tilde{w}_0^-$, we get

$$\begin{aligned}(\tilde{D}f)_0 &= \frac{6}{h^2}\left[(\tilde{w}^- f)_0' + \frac{h^2}{6}(\tilde{w}^- f)_0''' + \frac{h^4}{120}(\tilde{w}^- f)_0^{(5)} + \cdots\right] \\ &= 3\left[f_0' + \frac{h^2}{6}f_0''' - h^2 f_0' + \cdots\right].\end{aligned} \tag{A7}$$

To calculate all these derivatives, we used the continuum values $\tilde{w}^- = R^2/[2(1+R^2)]$ and $R^{(m)}(0) = 0$ for every integer $m > 1$. It is therefore clear that using Evans' method

at the origin is effectively the same as using l'Hôpital's rule there.

But now, we encounter a problem. If we use Sarbach's method to define $\tilde{D}$ for all $I \neq 0$ and at some instant $\Psi_I \approx R_I$ near the origin, then, from Eqs. (100) and (104), the associated error near the origin goes like $h^2/R^2 \approx h^2/r^2 = h^2/(I^2h^2) = 1/I^2$, which does not converge. Our strategy to overcome this problem is to use dissipation (as outlined in the following section). At the origin, we therefore simply use l'Hôpital's rule.

The choice $n = 2$ of the compactification parameter in Eq. (3) gives a nonzero weight to the $(\tilde{\sigma}^+)^2$ term at $r_{\mathscr{I}}$ in the energy defined by Eqs. (31) and (40), and hence to its discrete version, and makes the discrete energy a norm, so that the discrete energy has a positive weight at all grid points, with a possible exception at the origin. The origin has a positive weight whenever we use Evans' method to define $\tilde{D}$ there and has a zero weight whenever we rewrite the equations there using l'Hôpital's rule instead. In the latter case, we do not include the origin in our definition of discrete energy and define all the operators as $N \times N$ matrices over the space of the grid functions defined on the grid points $I = 1, \ldots, N$. Thus, the choice $n = 2$ still makes the discrete energy a norm.

APPENDIX B: FIXING UP THE ENERGY

The SBP-Stable scheme has been built for optimality in the energy given by Eq. (93). As it is built directly on the physical energy, this has the advantage that the resulting method satisfies a precise energy balance relation with $\dot{\hat{E}} \leq 0$. Unfortunately, however, in the massless case this physical energy is degenerate, in that the rescaled field $\tilde{\Psi}$ is completely absent. A similar degeneracy happens near $\mathscr{I}^+$ whenever the potential F falls off fast enough. Fortunately, we can easily adjust the energy, taking instead

$$\begin{aligned}\tilde{E} &= \hat{E} + \frac{1}{2}\Psi^T \Upsilon [r^2] \Psi \\ &= \frac{1}{2}[\tilde{\Psi}^T \Upsilon ([r^2] + F\tilde{W})\tilde{\Psi} + (\tilde{\Sigma}^+)^T \Upsilon \tilde{W}^+ \tilde{\Sigma}^+ \\ &\quad + (\tilde{\Sigma}^-)^T \Upsilon \tilde{W}^- \tilde{\Sigma}^-] \end{aligned} \tag{B1}$$

but keeping the exact same discretization as before. Using the Grönwall inequality, we easily obtain the estimate

$$\tilde{E}(t) \leq C(t_{\max})\tilde{E}(0), \tag{B2}$$

for all $0 \leq t \leq t_{\max}$ with $C(t_{\max}) > 0$ a constant independent of initial data for any $t_{\max}$. In other words, by sacrificing strict stability (working with this adjusted energy), we gain nondegenerate estimates, and, because we have not actually changed the discretization, we still have strict stability in the degenerate physical energy.

APPENDIX C: DISSIPATION OPERATOR

In this Appendix, we first give a brief discussion of standard dissipation operators before showing, in the second part, how these operators can be naturally included within our framework, both at the origin in spherical polar coordinates and near null infinity.

1. For 1D and in the trivial L^2 norm

We start by considering the fourth-order Kreiss-Oliger dissipation operator [52,62,63]

$$Q_{\mathrm{KO}} = -\epsilon h^3 h^{-4} (D_+ D_-)^2, \tag{C1}$$

where ϵ is the dissipation parameter whose value is set in our numerical evolutions. We will assume that we have an operator Q_d which agrees with this in the bulk of the grid and taking an alternative form to be fixed just at a small number of grid points near the boundaries. Ultimately, we will "thread" the weights present in our norms through this operator to render it suitable for use with the second-order accurate D and $\tilde{D}$ operators. Here,

$$(D_\pm f)_I = \pm \frac{f_{I\pm1} - f_I}{2} \tag{C2}$$

are the forward and backward finite-difference operators, denoted by plus and minus signs, respectively. This dissipation operator, which is centered, is defined only in the bulk and corresponds to the fourth-order derivative of a dynamical variable at second-order accuracy suppressed by a power of the grid spacing:

$$\begin{aligned}[h^{-4}(D_+D_-)^2 f]_I &= \frac{f_{I-2} - 4f_{I-1} + 6f_I - 4f_{I+1} + f_{I+2}}{h^4} \\ &= \left[f_I^{(4)} + \frac{h^2}{6} f_I^{(6)} + \cdots\right]. \end{aligned} \tag{C3}$$

Ideally, we wish to define Q_d at the outer boundary in such a way that the following desirable properties are satisfied:

(1) It satisfies the DP, as detailed momentarily.
(2) It should be h^3 times a discrete approximation of the fourth -order derivative, as in Eq. (C3), of the dynamical variable on which it acts.

The DP, as described in Ref. [37], is the requirement that, in the inner product that induces the norm used to establish stability, Q_d satisfies the inequality

$$(\Psi, Q_d \Psi) \leq 0, \tag{C4}$$

for any state vector Ψ. In this subsection, for simplicity, we assume that the state vector consists of a single grid function Ψ and work with the norm

$$(\Psi, \Psi)_\Upsilon = \Psi^T \Upsilon \Psi. \tag{C5}$$

The second desirable property assures that this operator vanishes like h^3 in the continuum limit. In other words, it assures that the dissipation term in each equation acts like a higher-order error associated with a finite-differencing scheme, which we want to match for every grid point.

We next consider the form that each of these properties alone gives to Q_d at the outer boundary. We denote the dissipation operator obtained by demanding the first property alone by Q_{d1} and that obtained from the second property alone by Q_{d2}. Presently, we do not know how, or if, both can be imposed simultaneously. We will ignore the coefficient ϵ in our calculations, as it plays no role there.

Substituting Eq. (C1) in the norm on the left of Eq. (C4), with the norm defined by Eq. (C5), gives

$$\Psi^T \Upsilon Q_d \Psi = -\|D^{(2)}\Psi\|^2 + (\text{boundary terms}), \tag{C6}$$

where

$$\|D^{(2)}\Psi\|^2 = (D^{(2)}\Psi)^T (D^{(2)}\Psi) \tag{C7}$$

is the trivial l^2 norm. Here, $D^{(2)}$ is a centered finite-difference operator which approximates the second-order derivative of a smooth function f projected on the grid at second-order accuracy and is defined as

$$(\Upsilon^{-2} D^{(2)} f)_I = \frac{f_{I-1} - 2f_I + f_{I+1}}{h^2} = f''_I + \frac{h^2}{12} f''''_I + \cdots \tag{C8}$$

in the bulk, and Υ is defined by Eq. (61), with $h_N = h/2$. The form of the first term on the right of Eq. (C6) is not surprising, because, in the continuum setting, we have

$$\begin{aligned}(f, f^{(4)}) &\equiv \int_0^{r_{\mathcal{J}}} f f'''' dr \\ &= \int_0^{r_{\mathcal{J}}} (f'')^2 dr + (f f''' - f' f'')|_0^{r_{\mathcal{J}}}.\end{aligned} \tag{C9}$$

The form of the boundary terms above will depend on the definition of Q_d at the boundary. In order to satisfy the DP, as defined by Eq. (C4), one possibility is to force the boundary terms to be identically zero. This leads to defining Q_{d1} from the equation $(\Psi, Q_{d1}\Psi) = -\|D^{(2)}\Psi\|^2$, to get

$$Q_{d1} = -\Upsilon^{-1} (D^{(2)})^T D^{(2)}. \tag{C10}$$

Here, $D^{(2)}$ is defined by Eq. (C8) for $I = 0, \ldots, N-1$. At the last grid point, we define $D^{(2)}$ as

$$(\Upsilon^{-2} D^{(2)} f)_N = \frac{f_{N-2} - 2f_{N-1} + f_N}{h^2} = f''_N + h f'''_N + \cdots. \tag{C11}$$

This gives

$$(D^{(2)} f)_N = \frac{f_{N-2} - 2f_{N-1} + f_N}{4}. \tag{C12}$$

The resulting Q_{d1} is the same as Eq. (C1) in the bulk and takes the following form at the outer boundary:

$$\begin{pmatrix} \cdot & \cdot & \cdot & \cdot & \cdot & \cdot & \cdot \\ \cdot & -\frac{6}{h} & \frac{4}{h} & -\frac{1}{h} & 0 & 0 & 0 \\ \cdot & \frac{4}{h} & -\frac{6}{h} & \frac{4}{h} & -\frac{1}{h} & 0 & 0 \\ \cdot & -\frac{1}{h} & \frac{4}{h} & -\frac{6}{h} & \frac{4}{h} & -\frac{1}{h} & 0 \\ \cdot & 0 & -\frac{1}{h} & \frac{4}{h} & -\frac{97}{16h} & \frac{33}{8h} & -\frac{17}{16h} \\ \cdot & 0 & 0 & -\frac{1}{h} & \frac{33}{8h} & -\frac{21}{4h} & \frac{17}{8h} \\ \cdot & 0 & 0 & 0 & -\frac{17}{8h} & \frac{17}{4h} & -\frac{17}{8h} \end{pmatrix}. \tag{C13}$$

With this definition, $Q_{d1} f \approx h^3 f^{(4)}$ in the bulk and is $\approx h f^{(2)}$ at the last three grid points. Therefore, it is expected that Q_{d1} affects the pointwise convergence at the last three grid points, at least in the TEM scheme, as it dominates the truncation error there, which is $\approx h^2 f^{(3)}$ for that scheme. There is no sense in incorporating the TEM property in the definition of $D^{(2)}$ in the construction of Q_{d1}, because doing so does not avoid these lower-order terms in the final operator.

If we instead prioritize the second desirable property when defining Q_d near the outer boundary, we need to redefine the operator only at the last two grid points. This property assures that the dissipation operator does not affect the pointwise accuracy of the numerical scheme at any grid point. We do not need to incorporate TEM to define this operator at the last two grid points, as it is already $O(h^3)$ and we ignored all the terms in our TEM discretization of order higher than h^3. Remember that we matched all the h^2 and h^3 coefficients in the finite-difference approximation D to the partial derivative ∂_r at all grid points to derive our TEM scheme. Demanding only that the dissipation operator should correspond to $h^3 f^{(4)}$ at its lowest order and ignoring the associated errors, we need only a five-point stencil to define it at the last two grid points. From this, we obtain

$$\begin{aligned}(Q_{d2} f)_{N-1} &= \epsilon h^{-1} (-f_{N-4} + 4f_{N-3} - 6f_{N-2} + 4f_{N-1} \\ &\quad - f_N) \\ &= -\epsilon h^3 [h^{-4} D_-^3 D_+ f]_{N-1}\end{aligned} \tag{C14}$$

and

$$\begin{aligned}(Q_{d2} f)_N &= \epsilon h^{-1} (-f_{N-4} + 4f_{N-3} - 6f_{N-2} + 4f_{N-1} - f_N) \\ &= -\epsilon h^3 [h^{-4} D_-^4 f]_N.\end{aligned} \tag{C15}$$

In this case, the operator Q_{d2} satisfies Eq. (C6), where the boundary terms are merely obtained from the difference between Q_{d2} and Q_{d1}, and we get

$$(\Psi, Q_{d2}\Psi)_\Upsilon = -\|D^{(2)}\Psi\|^2 + \left(-\Psi_{N-4}\Psi_{N-1} - \frac{\Psi_{N-4}\Psi_N}{2} + 5\Psi_{N-3}\Psi_{N-1} + 2\Psi_{N-3}\Psi_N + \frac{\Psi_{N-2}^2}{16} - \frac{41\Psi_{N-2}\Psi_{N-1}}{4} - \frac{15\Psi_{N-2}\Psi_N}{8} + \frac{37\Psi_{N-1}^2}{4} - \frac{13\Psi_{N-1}\Psi_N}{4} + \frac{9\Psi_N^2}{16}\right). \tag{C16}$$

It is not immediately clear if Q_{d2} satisfies the DP. Assuming that we are treating the initial data for which the TEM scheme is convergent, we can Taylor expand all Ψ_I's in the boundary term at the last grid point to obtain

$$(\Psi, Q_{d2}\Psi)_\Upsilon = -\|D^{(2)}\Psi\|^2 + O(h^3). \tag{C17}$$

Therefore, at sufficient resolution, we can make the h^3 term smaller such that only the bulk term, which is negative definite, dominates. In this weak sense Q_{d2} is still dissipative, even if it does not satisfy the DP.

2. In 3D, spherical polar coordinates, and energy norm

As we will be using the energy norm to perform our norm convergence tests, the next step is to construct a dissipation operator which satisfies the DP directly in our energy norm and in spherical polar coordinates. Since the weights of $\tilde{\Psi}$, $\tilde{\Sigma}^+$, and $\tilde{\Sigma}^-$ in our energy norm differ, we need to define these operators differently for each grid function. This needs to be done in such a way that a nontrivial dissipative effect is maintained on the solution at the origin itself. Our basic strategy is to take an operator Q_d known to satisfy the DP for a single grid function in the $(\cdot,\cdot)_\Upsilon$ norm used in the last section and then thread our weights into it. Schematically, this looks like $(W^{-1/2})Q_d(W^{1/2})$ away from the origin. Recalling that each $W \sim r^2$ near the origin, we use l'Hôpital's rule to regularize the operator there. The remaining subtlety to overcome is the parity of our evolved variables, which are a combination of even and odd quantities that makes the application of l'Hôpital's rule delicate for general fields. To see this, note, for example, that the second-order differential operator $\Delta\psi \equiv r^{-1}\partial_r^2(r\psi)$ is defined only on even functions, so a vector Laplace operator (or some such) is required.

We now outline the complete construction. We start by taking the DP operator Q_{d1} from before, now replacing the ϵ parameter. From this, we define two auxiliary operators

$$\hat{Q}_1 = Q_{d1}, \tag{C18}$$

which is well defined on odd grid functions, and

$$\hat{Q}_2 = [r]^T Q_{d1}[r], \tag{C19}$$

which is well defined on even grid functions. Both satisfy the DP using $(\cdot,\cdot)_\Upsilon$. The next question is, given $\hat{Q}_1$ and $\hat{Q}_2$, how to use them with our equations of motion. Considering our evolution system, we know that Ψ is an even function. Using the parity conditions (A2), we can also separate $\tilde{\Sigma}^+$ and $\tilde{\Sigma}^+$ into their even and odd parts with

$$\tilde{\Sigma}^+ = \frac{\tilde{\Sigma}^+ + \tilde{\Sigma}^-}{2} + \frac{\tilde{\Sigma}^+ - \tilde{\Sigma}^-}{2},$$
$$\tilde{\Sigma}^- = \frac{\tilde{\Sigma}^- + \tilde{\Sigma}^+}{2} + \frac{\tilde{\Sigma}^- - \tilde{\Sigma}^+}{2}. \tag{C20}$$

The first terms on the right are the even parts of $\tilde{\Sigma}^+$ and $\tilde{\Sigma}^-$, respectively, and the second their odd parts. Defining

$$\tilde{\Sigma}^e := \frac{\tilde{\Sigma}^+ + \tilde{\Sigma}^-}{2}, \qquad \tilde{\Sigma}^o := \frac{\tilde{\Sigma}^+ - \tilde{\Sigma}^-}{2}, \tag{C21}$$

we get

$$\tilde{\Sigma}^+ = \tilde{\Sigma}^e + \tilde{\Sigma}^o, \qquad \tilde{\Sigma}^- = \tilde{\Sigma}^e - \tilde{\Sigma}^o. \tag{C22}$$

Observe that the state vector $\mathbf{U}$ can be written as $\mathbf{U} = (\tilde{\Psi}, \tilde{\Sigma}^+, \tilde{\Sigma}^-)^T$ or as $\mathbf{V} := (\tilde{\Psi}, \tilde{\Sigma}^e, \tilde{\Sigma}^o)^T$. These two representations are related as $\mathbf{U} = \mathbf{TV}$, with

$$\mathbf{T} = \begin{pmatrix} 1 & 0 & 0 \\ 0 & 1 & 1 \\ 0 & 1 & -1 \end{pmatrix}. \tag{C23}$$

Observe that $\mathbf{T} = \hat{\mathbf{T}}\mathbf{\Lambda}$ with $\mathbf{\Lambda} = \mathrm{diag}(1, \sqrt{2}, \sqrt{2})$ and $\hat{\mathbf{T}}$ a symmetric, orthogonal matrix. The weight matrices in our energy norm satisfy the parity conditions

$$\tilde{W}(-r) = \tilde{W}(r) \quad \text{and} \quad \tilde{W}^\pm(-r) = \tilde{W}^\mp(r). \tag{C24}$$

Now, away from the origin, we can define the dissipation operator as

$$\mathbf{Q} = \mathbf{H}^{-1/2}\hat{\mathbf{T}}\mathbf{Q_d}\hat{\mathbf{T}}\mathbf{H}^{1/2}, \tag{C25}$$

with

$$\mathbf{Q_d} = \begin{pmatrix} \hat{Q}_1 & 0 & 0 \\ 0 & \hat{Q}_1 & 0 \\ 0 & 0 & \hat{Q}_2 \end{pmatrix}. \tag{C26}$$

At the origin, we simply apply l'Hôpital's rule which, as mentioned above, results in a regular operator. Crucial here is that $\mathbf{Q_d}$ satisfies the DP in the $(\cdot,\cdot)_\Upsilon$ norm. This definition guarantees that the dissipation operators respect the parity of the fields to which they are applied, because

$$\mathbf{T}^{-1}\mathbf{Q}\mathbf{U} = (\mathbf{T}^T\mathbf{H}^{1/2}\mathbf{T})^{-1}\mathbf{Q}_\mathbf{d}(\mathbf{T}^T\mathbf{H}^{1/2}\mathbf{T})\mathbf{V}, \tag{C27}$$

where both $\mathbf{Q_d}$, the matrix given in parentheses on the right, and its inverse respect parity. To verify that this choice satisfies the DP in our energy norm, we compute directly obtaining

$$\mathbf{U}^T\Upsilon\mathbf{H}\mathbf{Q}\mathbf{U} = (\hat{\mathbf{T}}\mathbf{H}^{1/2}\mathbf{U})^T\Upsilon\mathbf{Q}_\mathbf{d}(\hat{\mathbf{T}}\mathbf{H}^{1/2}\mathbf{U}) \leq 0, \tag{C28}$$

as desired. This requires the fact that $\mathbf{H}^{1/2}$ and $\hat{\mathbf{T}}$ commute with Υ, along with the other properties noted above. In our discretization, we *use* the operator by choosing

$$\frac{d}{dt}\mathbf{U} = \ldots + \mathbf{Q}\mathbf{U}, \tag{C29}$$

where the ellipses denote right-hand sides obtained solely from the earlier scheme. More explicitly, we can write this as

$$\begin{aligned}
\dot{\tilde{\Psi}} &= \cdots + ([r^2] + [F]\tilde{W})^{-1/2}\hat{Q}_1([r^2] + [F]\tilde{W})^{1/2}\tilde{\Psi},\\
\dot{\tilde{\Sigma}}^+ &= \cdots + \frac{1}{4}[(\tilde{W}^+)^{-1/2}(\hat{Q}_1 + \hat{Q}_2)(\tilde{W}^+)^{1/2}\tilde{\Sigma}^+ + (\tilde{W}^+)^{-1/2}(\hat{Q}_1 - \hat{Q}_2)(\tilde{W}^-)^{1/2}\tilde{\Sigma}^-],\\
\dot{\tilde{\Sigma}}^- &= \cdots + \frac{1}{4}[(\tilde{W}^-)^{-1/2}(\hat{Q}_1 - \hat{Q}_2)(\tilde{W}^+)^{1/2}\tilde{\Sigma}^+ + (\tilde{W}^-)^{-1/2}(\hat{Q}_1 + \hat{Q}_2)(\tilde{W}^-)^{1/2}\tilde{\Sigma}^-],
\end{aligned} \tag{C30}$$

with suitable application of l'Hôpital's rule understood at the origin. To derive this, we use the adjusted energy norm (B1). To see that the dissipation effectively removes energy from the system, we need only compute the time derivative of the energy norm, obtaining

$$\dot{\tilde{E}} = \cdots + \frac{1}{2}\mathbf{U}^T\mathbf{H}\Upsilon\mathbf{Q}\mathbf{U}, \tag{C31}$$

as desired. We close with the observation that the dissipation operator is not defined at all grid points for which FR' becomes unbounded, as is the case with LMKGE at $\mathscr{I}^+$. (Although, in that case, neither the SBP-Stable nor the SBP-TEM scheme are defined anyway.)

[1] R. Penrose, Phys. Rev. Lett. **10**, 66 (1963).
[2] N. T. Bishop, R. Gómez, L. Lehner, M. Maharaj, and J. Winicour, Phys. Rev. D **56**, 6298 (1997).
[3] N. T. Bishop, R. Gómez, L. Lehner, and J. Winicour, Phys. Rev. D **54**, 6153 (1996).
[4] Y. Zlochower, R. Gómez, S. Husa, L. Lehner, and J. Winicour, Phys. Rev. D **68**, 084014 (2003).
[5] C. J. Handmer and B. Szilagyi, Classical Quantum Gravity **32**, 025008 (2015).
[6] K. Barkett, J. Moxon, M. A. Scheel, and B. Szilágyi, Phys. Rev. D **102**, 024004 (2020).
[7] J. Winicour, Living Rev. Relativity **15**, 2 (2012).
[8] T. Giannakopoulos, D. Hilditch, and M. Zilhao, Phys. Rev. D **102**, 064035 (2020).
[9] H. Friedrich, Proc. R. Soc. A **375**, 169 (1981).
[10] H. Friedrich, Proc. R. Soc. A **378**, 401 (1981).
[11] V. Moncrief and O. Rinne, Classical Quantum Gravity **26**, 125010 (2009).
[12] A. Zenginoglu, Classical Quantum Gravity **25**, 195025 (2008).
[13] O. Rinne, Classical Quantum Gravity **27**, 035014 (2010).
[14] J. M. Bardeen, O. Sarbach, and L. T. Buchman, Phys. Rev. D **83**, 104045 (2011).
[15] A. Vañó-Viñuales, S. Husa, and D. Hilditch, Classical Quantum Gravity **32**, 175010 (2015).
[16] A. Vañó-Viñuales, Ph.D. thesis, U. Iles Balears, Palma (2015), arXiv:1512.00776, http://inspirehep.net/record/1407828/files/arXiv:1512.00776.pdf.
[17] D. Hilditch, E. Harms, M. Bugner, H. Rüter, and B. Brügmann, Classical Quantum Gravity **35**, 055003 (2018).
[18] D. Hilditch, arXiv:1509.02071.
[19] E. Gasperin and D. Hilditch, Classical Quantum Gravity **36**, 195016 (2019).
[20] E. Gasperin, S. Gautam, D. Hilditch, and A. Vañó-Viñuales, Classical Quantum Gravity **37**, 035006 (2020).
[21] A. Zenginoglu, J. Comput. Phys. **230**, 2286 (2011).
[22] A. Zenginoglu, Phys. Rev. D **83**, 127502 (2011).
[23] B. Strand, J. Comput. Phys. **110**, 47 (1994).
[24] F. Pretorius, Classical Quantum Gravity **22**, 425 (2005).
[25] J. Winicour, J. Math. Phys. (N.Y.) **29**, 2117 (1988).
[26] G. Calabrese, C. Gundlach, and D. Hilditch, Classical Quantum Gravity **23**, 4829 (2006).
[27] C. Gundlach, J. M. Martin-Garcia, G. Calabrese, and I. Hinder, Classical Quantum Gravity **22**, 3767 (2005).
[28] L. Lindblom, M. A. Scheel, L. E. Kidder, R. Owen, and O. Rinne, Classical Quantum Gravity **23**, S447 (2006).

[29] L. Hörmander, *Lectures on Nonlinear Hyperbolic Differential Equations*, Mathématiques et Applications (Springer, Berlin, 1997).
[30] H. Lindblad and I. Rodnianski, arXiv:math/0411109.
[31] C. R. Evans, Ph.D. thesis, University of Texas at Austin, 1984.
[32] G. Calabrese and D. Neilsen, Phys. Rev. D **71**, 124027 (2005).
[33] D. Neilsen, L. Lehner, O. Sarbach, and M. Tiglio, Lect. Notes Phys. **692**, 223 (2006).
[34] S. Aretakis, https://www.math.toronto.edu/aretakis/General%20Relativity-Aretakis.pdf (2013).
[35] G. Calabrese, L. Lehner, D. Neilsen, J. Pullin, O. Reula, O. Sarbach, and M. Tiglio, Classical Quantum Gravity **20**, L245 (2003).
[36] G. Calabrese and D. Neilsen, Phys. Rev. D **69**, 044020 (2004).
[37] G. Calabrese, L. Lehner, O. Reula, O. Sarbach, and M. Tiglio, Classical Quantum Gravity **21**, 5735 (2004).
[38] J. Seiler, B. Szilagyi, D. Pollney, and L. Rezzolla, Classical Quantum Gravity **25**, 175020 (2008).
[39] N. W. Taylor, L. E. Kidder, and S. A. Teukolsky, Phys. Rev. D **82**, 024037 (2010).
[40] O. Sarbach and M. Tiglio, Living Rev. Relativity **15**, 9 (2012).
[41] J. G. Baker, J. Centrella, D.-I. Choi, M. Koppitz, and J. van Meter, Phys. Rev. Lett. **96**, 111102 (2006).
[42] M. Campanelli, C. O. Lousto, P. Marronetti, and Y. Zlochower, Phys. Rev. Lett. **96**, 111101 (2006).
[43] T. W. Baumgarte and S. L. Shapiro, Phys. Rev. D **59**, 024007 (1998).
[44] M. Shibata and T. Nakamura, Phys. Rev. D **52**, 5428 (1995).
[45] T. Nakamura, K. Oohara, and Y. Kojima, Prog. Theor. Phys. Suppl. **90**, 1 (1987).
[46] C. Bona, T. Ledvinka, C. Palenzuela, and M. Žáček, Phys. Rev. D **67**, 104005 (2003).
[47] S. Bernuzzi and D. Hilditch, Phys. Rev. D **81**, 084003 (2010).
[48] D. Alic, C. Bona-Casas, C. Bona, L. Rezzolla, and C. Palenzuela, Phys. Rev. D **85**, 064040 (2012).
[49] J. Thomas, *Numerical Partial Differential Equations: Finite Difference Methods*, Texts in Applied Mathematics (Springer, New York, 1998), ISBN 9780387979991, https://books.google.pt/books?id=op5COPwUfX8C.
[50] C. Gundlach, J. M. Martin-Garcia, and D. Garfinkle, Classical Quantum Gravity **30**, 145003 (2013).
[51] F. Pretorius, Ph. D. thesis, Department of Physics and Astronomy, The University of British Columbia, 2002, http://laplace.physics.ubc.ca/Theses/Phd/pretorius.pdf.
[52] B. Gustafsson, H.-O. Kreiss, and J. Oliger, *Time Dependent Problems and Difference Methods* (Wiley, New York, 1995).
[53] A. Vañó-Viñuales and S. Husa, Classical Quantum Gravity **35**, 045014 (2018).
[54] R. Price, Phys. Rev. D **5**, 2419 (1972).
[55] S. Klainerman, Commun. Pure Appl. Math. **46**, 137 (1993).
[56] M. Chirvasa and S. Husa, J. Comput. Phys. **229**, 2675 (2010).
[57] K. Duru, F. Fung, and C. Williams, arXiv:2011.02600.
[58] D. Alic, C. Bona, and C. Bona-Casas, Phys. Rev. D **79**, 044026 (2009).
[59] J. D. Brown, P. Diener, S. E. Field, J. S. Hesthaven, F. Herrmann, A. H. Mroué, O. Sarbach, E. Schnetter, M. Tiglio, and M. Wagman, Phys. Rev. D **85**, 084004 (2012).
[60] J. M. Miller and E. Schnetter, Classical Quantum Gravity **34**, 015003 (2017).
[61] M. Dumbser, F. Guercilena, S. Köppel, L. Rezzolla, and O. Zanotti, Phys. Rev. D **97**, 084053 (2018).
[62] H. O. Kreiss and J. Oliger, *Methods for the Approximate Solution of Time Dependent Problems* (GARP Publication Series No. 10, Geneva, 1973).
[63] H.-O. Kreiss and J. Lorenz, *Initial-Boundary Value Problems and the Navier-Stokes Equations* (Academic Press, New York, 1989).